



Regional variation in the effectiveness of methane-based and land-based climate mitigation options

Garry D. Hayman^{1,*}, Edward Comyn-Platt¹, Chris Huntingford¹, Anna B. Harper², Tom Powell², Peter M. Cox², William Collins³, Christopher Webber³, Jason Lowe^{4,5}, Stephen Sitch², Joanna I. House⁶, Jonathan C. Doelman⁷, Detlef P. van Vuuren^{7,8}, Sarah E. Chadburn², Eleanor Burke⁵, Nicola Gedney⁹.

¹ Centre for Ecology & Hydrology, Wallingford, OX10 8BB, U.K.

² University of Exeter, Exeter, EX4 4QF, U.K.

³ University of Reading, Reading, RG6 6BB, U.K.

⁴ University of Leeds, Leeds, LS2 9JT, U.K.

10 ⁵ Met Office Hadley Centre, FitzRoy Road, Exeter, EX1 3PB, U.K.

⁶ Cabot Institute for the Environment, University of Bristol, Bristol, BS8 1SS, U.K.

⁷ Department of Climate, Air and Energy, Netherlands Environmental Assessment Agency (PBL), PO Box 30314, 2500 GH The Hague, Netherlands

⁸ Copernicus Institute of Sustainable Development, Utrecht University, Heidelberglaan 2, 3584 CS, the Netherlands

15 ⁹ Met Office Hadley Centre, Joint Centre for Hydrometeorological Research, Wallingford, OX10 8BB, U.K.

Correspondence to: Garry Hayman (garr@ceh.ac.uk)

Abstract. Scenarios avoiding global warming greater than 1.5 or 2°C, as stipulated in the Paris Agreement, may require the combined mitigation of anthropogenic greenhouse gas emissions alongside enhancing negative emissions through approaches such as afforestation/reforestation (AR) and biomass energy with carbon capture and storage (BECCS). We use the JULES
20 land-surface model coupled to an inverted form of the IMOGEN climate emulator to investigate mitigation scenarios that achieve the 1.5 or 2°C warming targets of the Paris Agreement. Specifically, we characterise the global and regional effectiveness of land-based (BECCS and/or AR) and anthropogenic methane (CH₄) emission mitigation, separately and in combination, on the anthropogenic fossil fuel carbon dioxide emission budgets (AFFEBs) to 2100, using consistent data and socio-economic assumptions from the IMAGE integrated assessment model. The analysis includes the effects of the methane
25 and carbon-climate feedbacks from wetlands and permafrost thaw, which we have shown previously to be significant constraints on the AFFEBs.

Globally, mitigation of anthropogenic CH₄ emissions has large impacts on the anthropogenic fossil fuel emission budgets, potentially offsetting (i.e. allowing extra) carbon dioxide emissions of 188-212 GtC. Methane mitigation is beneficial everywhere, particularly for the major CH₄-emitting regions of India, USA and China. Land-based mitigation has the potential
30 to offset 51-100 GtC globally, but both the effectiveness and the preferred land-management strategy (i.e., AR or BECCS) have strong regional dependencies. Additional analysis shows extensive BECCS could adversely affect water security for several regions. Our results highlight the extra potential CO₂ emissions that can occur, while still keeping global warming below key warming thresholds, by investment in regionally appropriate mitigation strategies.



35 1 Introduction

The stated aims of the Paris Agreement of the United Nations Framework Convention on Climate Change (UNFCCC, 2015) are “to hold the increase in global average temperature to well below 2°C and to pursue efforts to limit the increase to 1.5°C”. The global average surface temperature for the decade 2006-2015 was 0.87°C above pre-industrial levels and is likely to reach 1.5°C between the years 2030 and 2052, if global warming continues at current rates (IPCC, 2018). Meeting the Paris Agreement goals will, therefore, require sustained reductions in sources of long-lived anthropogenic greenhouse gases (GHGs) and some short-lived climate forcers (SLCFs) such as methane, alongside increasingly extensive implementations of carbon dioxide removal (CDR) technologies. Accurate information is needed on the range and efficacy of options available to achieve this.

Biomass energy with carbon capture and storage (BECCS) and afforestation/reforestation (AR) are the most widely considered CDR technologies in the climate and energy literature. For scenarios consistent with a 2°C warming target, the review by Smith et al. (2016) finds this may require (1) a median removal of 3.3 GtC yr⁻¹ from the atmosphere through BECCS by 2100 and (2) a mean CDR through AR of 1.1 GtC yr⁻¹ by 2100, giving a total CDR equivalent to 47% of present-day emissions from fossil fuel and other industrial sources (Le Quéré et al., 2018). Although there are fewer scenarios that look specifically at the 1.5°C pathway, BECCS is still the major CDR approach (Rogelj et al., 2018). For the default assumptions in Fuss et al. (2018), BECCS would remove a median of 4 GtC yr⁻¹ by 2100 and a total of 41-327 GtC from the atmosphere during the twenty-first century, equivalent to about 4-30 years of current annual emissions. The land requirements for BECCS will be greater for the 1.5°C target, although published estimates are similar for the two warming targets, with between 380-700 Mha required for the 2°C target (Smith et al., 2016) and greater than 600 Mha for the 1.5°C target (van Vuuren et al., 2018). Other key differences are the start date of implementation and the rate of deployment. While the CDR figures assume optimism about the mitigation potential of BECCS, concerns have been raised about the potentially detrimental impacts of BECCS on food production, water availability and biodiversity, e.g., (Krause et al., 2017; Heck et al., 2018). Others note the risks and query the feasibility of large-scale deployment of BECCS e.g. (Anderson and Peters, 2016; Vaughan and Gough, 2016; Vaughan et al., 2018). The IPCC Special Report “Climate Change and Land Use”(IPCC, 2019) provides a further synthesis and perspective on BECCS.

Harper et al. (2018) find the overall effectiveness of BECCS to be strongly dependent on the assumptions concerning yields, the use of initial above-ground biomass that is replaced and the calculated fossil-fuel emissions that are offset in the energy system. Notably, if BECCS involves replacing ecosystems that have higher carbon contents than energy crops, then AR and avoided deforestation can be more efficient than BECCS for atmospheric CO₂ removal over this century (Harper et al., 2018).

Mitigation of the anthropogenic emissions of non-CO₂ GHGs such as methane (CH₄) and of SLCFs such as black carbon have been shown to be attractive strategies with the potential to reduce projected global mean warming by 0.22-0.5°C by 2050 (Shindell et al., 2012; Stohl et al., 2015). It should be noted that these were based on scenarios with continued use of fossil



70 fuels. Through the link to tropospheric ozone (O_3), there are additional co-benefits of CH_4 mitigation for air quality, plant productivity and food production (Shindell et al., 2012) and carbon sequestration (Oliver et al., 2018). Control of anthropogenic CH_4 emissions leads to rapid decreases in its atmospheric concentration, with an approximately 9-year removal lifetime, and as such is an SLCF. Furthermore, many CH_4 mitigation options are inexpensive or even cost negative through the co-benefits achieved (Stohl et al., 2015), although expenditure becomes substantial at high levels of mitigation (Gernaat et al., 2015). The extra “allowable” carbon emissions from CH_4 mitigation can make a substantial difference to the feasibility or otherwise of achieving the Paris climate targets (Collins et al., 2018).

75 Some increases in atmospheric CH_4 are not related to direct anthropogenic activity, but indirectly to climate change triggering natural carbon and methane-climate feedbacks. These effects could act as positive feedbacks, and thus in the opposite direction to the mitigation of anthropogenic methane sources. Wetlands are the largest natural source of methane to the atmosphere and these emissions respond strongly to climate change (Melton et al., 2013; Gedney et al., 2019). A second natural feedback is from permafrost thaw. In a warming climate, the resulting microbial decomposition of previously frozen organic carbon is potentially one of the largest feedbacks from terrestrial ecosystems (Schoor et al., 2015). As the carbon and CH_4 climate feedbacks from natural wetlands and permafrost thaw could be substantial, this causes a reduction in anthropogenic CO_2 emission budgets compatible with climate change targets (Comyn-Platt et al., 2018; Gasser et al., 2018).

80 For the first time, we combine these elements (land-based mitigation, anthropogenic CH_4 mitigation, and natural carbon and methane climate feedbacks) in a climate/Earth System modelling framework. In contrast to previous studies, we use a process-based land surface model to assess these mitigation options by region, yielding policy-relevant information on the optimal mitigation strategy. Sect. 2 provides a brief description of the models, the experimental set-up and the key datasets used in the model runs and subsequent analysis. Sect. 3 presents and discusses the results, starting with a global perspective before addressing the regional dimension. For BECCS, we additionally investigate the sensitivity to key assumptions and consider the implications for water security. Sect. 4 contains our conclusions.

90 2 Approach and Methodology

Figure 1 shows a schematic of our approach, the workflow and the prescribed data used. We use the Joint UK Land-Environment Simulator (JULES, Sect. 2.1) (Best et al., 2011; Clark et al., 2011), coupled with an inverted form of the “Integrated Model Of Global Effects of climatic aNomalies” (IMOGEN, Sect. 2.2) (Comyn-Platt et al., 2018; Huntingford et al., 2010). IMOGEN is an intermediate complexity climate model, which uses “pattern scaling” to emulate 34 models in the CMIP5 ensemble. In the inverted form used here, IMOGEN follows a prescribed temperature pathway (Sect. 2.2.2). We derive the overall radiative forcing consistent with this temperature pathway using an energy balance model, including a simplified model of ocean uptake (of energy and CO_2). Using a combination of calculated and prescribed time series of annual radiative forcings, we derive the atmospheric CO_2 radiative forcing and hence its concentration, taking account of any land and ocean feedbacks. For the mitigation scenarios considered (Sect 2.3), we use consistent and compatible time series of (a)



100 anthropogenic methane emissions, (b) prescribed land areas for crops and BECCS (where relevant) and (c) radiative forcings for SLCFs and non-CO₂ GHGs (except CH₄), from the IMAGE integrated assessment model. In a post-processing step (Sect. 2.4.1), we take the modelled carbon stores for land (=vegetation and soil carbon), atmosphere and oceans from the IMOGEN-JULES output and calculate the anthropogenic fossil fuel emission budgets (AFFEB) compatible with the warming pathway. For the land-based scenarios involving BECCS, we optimise the AFFEB by selecting the greater land carbon uptake from the
105 'BECCS' or the variant 'natural' (i.e., no BECCS) scenario, for those grid cells where BECCS is deployed (Sect. 2.4.2). Further, we investigate the sensitivity of the optimisation to the assumption made about BECCS productivity and carbon uptake (Sect. 2.4.3). Section 2.5 lists the model runs undertaken and the key assumptions and datasets used.

2.1 The JULES model

We use the JULES land surface model (Best et al., 2011; Clark et al., 2011), release version 4.8, but with a number of
110 additions required specifically for our analysis:

1. Land use: We adopt the approach used by Harper et al. (2018) and prescribe *managed* land-use and land-use change (LULUC). On land used for agriculture, C3 and C4 grasses are allowed to grow to represent crops and pasture. The land-use mask consists of an annual fraction of agricultural land in each grid cell. Historical LULUC is based on the HYDE 3.1 dataset (Klein Goldewijk et al., 2011), and future LULUC is based on two scenarios (SSP2 RCP-1.9 and
115 SSP2 baseline), which were developed for use in the IMAGE integrated assessment model (IAM) (Doelman et al., 2018; van Vuuren et al., 2017) (see also Sect. 2.3).

Natural vegetation is represented by nine plant functional types (PFTs): broadleaf deciduous trees, tropical broadleaf evergreen trees, temperate broadleaf evergreen trees, needle-leaf deciduous trees, needle-leaf evergreen trees, C3 and C4 grasses, deciduous and evergreen shrubs (Harper et al., 2016). These PFTs are in competition for space in the non-agricultural fraction of grid cells, based on the TRIFFID (Top-down Representation of Interactive Foliage and Flora Including Dynamics) dynamic vegetation module within JULES (Clark et al., 2011). A further four PFTs are used to represent agriculture (C3 and C4 crops, and C3 and C4 pasture), and harvest is calculated separately for food and bioenergy crops (see Sect. 2.4.3, where we describe the modelling of carbon removed via bioenergy with CCS). When natural vegetation is converted to managed agricultural land, the vegetation carbon removed is placed into woody
120 product pools that decay at various rates back into the atmosphere (Jones et al., 2011). Hence, the carbon flux from LULUC is not lost from the system. There are also four non-vegetated surface types: urban, water, bare soil and ice.

2. Soil carbon: Following Comyn-Platt et al. (2018), we also use a 14 layered soil column for both hydro-thermal (Chadburn et al., 2015) and carbon dynamics (Burke et al., 2017a). Burke et al. (2017b) demonstrated that modelling the soil carbon fluxes as a multi-layered scheme improves estimates of soil carbon stocks and net ecosystem exchange.
130 In addition to the vertically discretised respiration and litter input terms, the soil-carbon balance calculation also includes a diffusivity term to represent cryoturbation/bioturbation processes. The freeze-thaw process of



135 cryoturbation is particularly important in cold permafrost-type soils (Burke et al., 2017b). Following Burke et al. (2017a), we diagnose permafrost wherever the deepest soil layer is below 0°C (assuming that this layer is below the depth of zero annual amplitude). Further, for permafrost regions, there is an additional variable to trace or diagnose “old” carbon and its release from permafrost as it thaws.

The multi-layered methanogenesis scheme improves the representation of high latitude methane emissions, where previous studies underestimated production at cold permafrost sites during “shoulder seasons” (Zona et al., 2016). Figure 2 shows the annual cycle in the observed and modelled wetland methane emissions at the Samoylov Island field site (panel a) and a comparison of observed and modelled annual mean fluxes at this and other sites (panel b).

140 The range of uncertainty used in our study (JULES low Q_{10} - JULES high Q_{10}) captures the range of uncertainty in the observations. Further, the layered methane scheme used in this work gives a better description of the shoulder season emissions when compared with the original, non-layered methane scheme in JULES. The multi-layered scheme allows an insulated sub-surface layer of active methanogenesis to continue after the surface has frozen. These model developments not only improve the seasonality of the emissions, but more importantly for this study capture the release of carbon as CH₄ from deep soil layers, including thawed permafrost. Further evaluation of the multi-layer 145 scheme can be found in Chadburn et al. (2020).

3. **Methane from wetlands:** Following Comyn-Platt et al. (2018), we also use the multi-layered soil carbon scheme described in (2) above to give the local land-atmosphere CH₄ flux, E_{CH_4} (kg C m⁻² s⁻¹):

$$E_{CH_4} = k \cdot f_{wetl} \cdot \sum_{i=1}^n C_s^{pools} \kappa_i \cdot \sum_{z=0m}^{z=3m} e^{-\gamma z} C_{S_{i,z}} \cdot Q_{10}(T_{soil_z})^{0.1(T_{soil_z}-T_0)} \quad (1)$$

150 where z is the depth in soil column (in m), i is the soil carbon pool, f_{wetl} (-) is the fraction of wetland area in the grid cell, κ_i (s⁻¹) is the specific respiration rate of each pool (Table 8 of Clark et al. (2011)), C_s (kg m⁻²) is soil carbon, T_{soil} (K) is the soil temperature. The decay constant γ (= 0.4 m⁻¹) describes the reduced contribution of CH₄ emission at deeper soil layers due to inhibited transport and increased oxidation through overlaying soil layers. This representation of inhibition and of the pathways for methane release to the atmosphere (e.g., by diffusion, ebullition and vascular transport) is a simplification. However, previous work which explicitly represented these processes showed little to 155 no improvement when compared with in-situ observations (McNorton et al., 2016). We do not model methane emissions from freshwater lakes (and oceans).

Comyn-Platt et al. (2018) varied Q_{10} in Eq. 1 to encapsulate a range of methanogenesis process uncertainty. They derive Q_{10} values for each GCM configuration to represent two wetland types identified in Turetsky et al. (2014) 160 (‘poor-fen’ and ‘rich-fen’). They also include a third ‘low- Q_{10} ’, which gives increased importance to high latitude emissions. Their ensemble spread was able to describe the magnitude and distribution of present-day CH₄ emissions from natural wetlands, according to the models used in the then-current global methane assessment (Saunio et al.,



2016). Here, we use the ‘low- Q_{10} ’ value of Comyn-Platt et al. (2018) (=2.0) and adopt a ‘high- Q_{10} ’ value of ~4.8 from the rich-fen parameterisation. The two Q_{10} values used here still capture the full range of the methanogenesis process uncertainty.

- 165
4. **Ozone vegetation damage:** We use a JULES configuration including ozone deposition damage to plant stomata, which affects land-atmosphere CO_2 exchange (Sitch et al., 2007). JULES requires surface atmospheric ozone concentrations, O_3 (ppb), for the duration of the simulation period (1850-2100). As in Collins et al. (2018), we take two sets of monthly near-surface O_3 concentration fields calculated using the HADGEM3-A GA4.0 model for low (1285 ppbv) and high (2062 ppbv) global mean atmospheric CH_4 concentrations (Stohl et al., 2015). We regrid these fields (1.875°x1.25° horizontal grid) to the spatial grid of IMOGEN-JULES (3.75°x2.5° horizontal grid). We then linearly interpolate between the respective months in the regridded O_3 fields using the global annual atmospheric CH_4 concentration. We use the CH_4 concentration profile from the prescribed SSP2_RCP-1.9_IMAGE scenario, adjusted for natural methane sources (see 3 above). We undertake runs using both the ‘high’ and ‘low’ vegetation ozone-damage parameter sets (Sitch et al., 2007).
- 170
- 175

2.2 The IMOGEN intermediate complexity climate model

2.2.1 IMOGEN

The IMOGEN climate impacts model (Huntingford et al., 2010) uses “pattern-scaling” to estimate changes to the seven meteorological variables required to drive JULES. Huntingford et al. (2010) assume that changes in local temperature, precipitation, humidity, wind-speed, surface shortwave and longwave radiation and pressure are linear in global warming. Spatial patterns of each variable (based on the 34 GCM simulations in CMIP5 (Comyn-Platt et al., 2018)) are multiplied by the amount of global warming over land, ΔT_L , to give local monthly predictions of climate change. When using IMOGEN in forward mode, ΔT_L is calculated with an Energy Balance Model (EBM) as a function of the overall changes in radiative forcing, ΔQ ($W\ m^{-2}$). The EBM includes a simple representation of the ocean uptake of heat and CO_2 . ΔQ is the sum of the atmospheric greenhouse gas contributions (Eq. 2) (Etminan et al., 2016), which in the forward mode are either calculated (CO_2 and CH_4) or prescribed (for other atmospheric contributors) on a yearly time step.

180

185

$$\Delta Q(total) = \Delta Q(CO_2) + \Delta Q(non\ CO_2\ GHGs) + \Delta Q(aerosols\ and\ other\ climate\ forcers) \quad (2)$$

Our simulations include a CH_4 feedback system that captures the climate impacts on CH_4 emissions from natural wetland sources. The approach used here follows Comyn-Platt et al. (2018) and Gedney et al. (2019), where the prescribed atmospheric methane concentrations, which assume a constant annual wetland CH_4 emission (van Vuuren et al., 2017), are modified using the anomaly in the modelled annual wetland CH_4 emission. The increased/reduced atmospheric CH_4 concentration will have a corresponding faster/slower atmospheric decay rate than the prescribed concentration pathway. We account for this following the approach of Cubasch et al. (2001). Related changes in atmospheric radiative forcing, in response to altered atmospheric

190



195 CH₄ concentrations, are calculated using the formulation from Etminan et al. (2016). We also include the indirect effect of these CH₄ emission changes on the forcing by tropospheric ozone and stratospheric water vapour by multiplying the CH₄ forcing by 1.65, based on Myhre et al. (2013).

In this study, we use the inverse version of IMOGEN, which follows prescribed temperature pathways (Fig. 3(a)). Comyn-Platt et al. (2018) describe the changes made to the EBM to create the inverse version. Each of the 34 GCMs that IMOGEN emulates has a different set of EBM parameters. Hence each GCM has a different time-evolving radiative forcing (ΔQ) estimate for a given temperature pathway, $\Delta T_G(t)$. When IMOGEN is forced with a historical record of ΔT_G , the range of ΔQ for the near present day (year 2015) from the 34 GCMs is 1.13 W m^{-2} . To ensure a smooth transition to the modelled future, we require the historical period, 1850-2015, to match observations of both ΔT_G and atmospheric composition for all GCMs. We, therefore, attribute the spread in ΔQ to the uncertainty in the non-CO₂ radiative forcing component, particularly the atmospheric aerosol contribution which has an uncertainty range of -0.5 to -4 Wm^{-2} (Stocker et al., 2013). Apart from our modelled CH₄ and CO₂ radiative forcings and the potential future balances between them, we use the projections from the IMAGE SSP2 baseline or RCP1.9 scenario for the radiative forcing of other atmospheric contributors (Fig. 3(b)).

2.2.2 Temperature Profile Formulation

Huntingford et al. (2017) a framework to create trajectories of global temperature increase, based on two parameters, and which model the efforts of humanity to limit emissions and, if necessary, capture atmospheric carbon. These profiles have the mathematical form of:

$$\Delta T(t) = \Delta T_0 + \gamma t - (1 - e^{-\mu(t)t})[\gamma t - (\Delta T_{Lim} - \Delta T_0)] \quad (3)$$

where $\Delta T(t)$ is the change in temperature from pre-industrial levels at year t , ΔT_0 is the temperature change at a given initial point (in this case $\Delta T_0 = 0.89^\circ\text{C}$ for 2015), ΔT_{Lim} is the final prescribed warming limit and

$$\mu(t) = \mu_0 + \mu_1 t \text{ and } \gamma = \beta - \mu_0(\Delta T_{Lim} - \Delta T_0) \quad (4)$$

215 where β ($= 0.00128$) is the current rate of warming and μ_0 and μ_1 are tuning parameters which describe anthropogenic attempts to stabilise global temperatures (Huntingford et al., 2017). The parameter values used for the two profiles are: (a) 1.5°C profile: $\Delta T_{lim} = 1.5^\circ\text{C}$; $\mu_0 = 0.1$ and $\mu_1 = 0.0$; (b) 2°C profile: $\Delta T_{lim} = 2^\circ\text{C}$; $\mu_0 = 0.08$ and $\mu_1 = 0.0$.

2.3 Methane and land-based mitigation scenarios

We use future projections of atmospheric CH₄ concentrations and LULUC from the IMAGE SSP2 projections (Doelman et al., 2018), for both the methane and land-use mitigation strategies. This ensures that all projections are consistent and based on the same set of IAM model and socio-economic pathway assumptions. The SSP2 socio-economic pathway is described as middle of the road (O'Neill et al., 2017), with social, economic, and technological trends largely following historical patterns



observed over the past century. Global population growth is moderate and levels off in the second half of the century. The intensity of resource and energy use declines. We define the upper and lower limits of anthropogenic mitigation as the lowest (RCP1.9) and highest (“baseline”) total radiative forcing pathways, respectively, within the IMAGE SSP2 ensemble (Riahi et al., 2017). We denote the RCP1.9 pathway as IM-1.9 and the “baseline” pathway as IM-BL.

The anthropogenic CH₄ emission increase from 318 Tg per annum in 2005 to 484 Tg per annum in 2100 in the IMAGE SSP2 baseline scenario, but fall to 162 Tg per annum in 2100 in the IMAGE SSP2 RCP1.9 scenario. The sectoral methane emissions in 2005 (Energy Supply & Demand: 113; Agriculture: 136; Other Land Use (primarily burning): 18; Waste 52, all in Tg per annum) are in agreement with the latest estimates of the global methane cycle (Saunio et al., 2019). As summarised in Supplementary Information, Table SI.1, the reduction in emissions from specific source sectors is achieved as follows: (a) coal production by maximising methane recovery from underground mining of hard coal; (b) oil/gas production & distribution, through control of fugitive emissions from equipment and pipeline leaks, and from venting during maintenance and repair; (c) enteric fermentation, through change in animal diet and the use of more productive animal types; (d) animal waste by capture and use of the methane emissions in anaerobic digesters; (e) wetland rice production, through changes to the water management regime and to the soils to reduce methanogenesis; (f) landfills by reducing the amount of organic material deposited and by capture of any methane released; (g) sewage and wastewater, through using more wastewater treatment plants and also recovery of the methane from such plants, and through more aerobic wastewater treatment. The levels of reduction vary between sectors, from 50% (agriculture) to 90% (fossil-fuel extraction and delivery). The abatement costs are between US\$ 300-1000 (1995 US\$) (Supplementary Information, Table SI.1). Figure 4 presents the IMAGE baseline and RCP1.9 CH₄ emission pathways globally and for selected IMAGE regions, including the major-emitting regions of India, USA and China (Supplementary Information, Figure SI.1 shows the emission pathways for all 26 IMAGE regions).

The IM-BL LULUC scenario assumes (a) moderate land-use change regulation; (b) moderately effective land-based mitigation; (c) the current preference for animal products; (d) moderate improvement in livestock efficiencies; and (e) moderate improvement in crop yields (Table 1 in (Doelman et al., 2018)). It represents a control scenario within which agricultural land is accrued to feed growing populations associated with the SSP2 pathway and with no deployment of BECCS. Three types of land-based climate change mitigation are implemented in the IMAGE land use mitigation scenarios (Doelman et al., 2018): (1) bioenergy; (2) reducing emissions from deforestation and degradation (REDD or avoided deforestation); and (3) reforestation of degraded forest areas. For the IM-1.9 scenario, there are high levels of REDD and full reforestation. The scenario assume a food-first policy (Daioglou et al., 2019) so that bioenergy crops are only implemented on land not required for food production (e.g., abandoned agricultural crop land). The demand for bioenergy is linked to the carbon price required to reach the mitigation target (Hoogwijk et al., 2009). In this scenario, the area of land used for bioenergy crops expands rapidly from 2030 to 2050, reaching a maximum of 550 Mha in 2060, and then declining to 430 Mha by 2100. Table 1 gives the maximum area of BECCS deployed in each IMAGE region for the IM-1.9 scenario.

We define a third LULUC pathway, which is identical to the IM-1.9 pathway, except that any land allocated to bioenergy crops is allocated instead to natural vegetation, i.e., areas of natural land, which are converted to bioenergy crops, remain as



natural vegetation, and areas, which are converted from food crops or pasture to bioenergy crops, return to natural vegetation. We denote this scenario as IM-1.9N. Table 1 also summarises the main differences in land use between the IM-1.9 and IM-1.9N scenarios for each IMAGE region.

260 Figure 3(c)-(h) present the effect of these scenarios on the modelled atmospheric CH₄ and CO₂ concentrations. We adjust the prescribed atmospheric CH₄ concentrations to allow for interannual variability in the wetland CH₄ emissions, as described in Sect. 2.2.1. The major control on the modelled atmospheric CH₄ concentrations is the methane emission pathway followed, with the temperature pathway (1.5° versus 2°C warming) having a minor effect. For CO₂, on the other hand, the temperature and the methane emission pathways both lead to increased atmospheric CO₂ concentrations, with the temperature pathway
 265 having a slightly larger effect.

2.4 Post-processing

2.4.1 Anthropogenic Fossil Fuel Emission Budget and Mitigation Potential

Following Comyn-Platt et al. (2018), we define the anthropogenic fossil fuel emission budget (AFFEB) for scenario i as the change in carbon stores from present to the year 2100:

$$270 \quad AFFEB_i = [C^{land}(2100) - C^{land}(2015)]_i + [C^{ocean}(2100) - C^{ocean}(2015)]_i \\ + [C^{atmos}(2100) - C^{atmos}(2015)]_i + BECCS(2015:2100)_i \quad (5)$$

where $C^{land}(t)$, $C^{ocean}(t)$ and $C^{atmos}(t)$ are the carbon stored in the land, ocean and atmosphere, respectively, in year t and $BECCS(t_1:t_2)$ is the carbon sequestered via BECCS between the years t_1 and t_2 . For brevity in the subsequent discussion, we use the following shorthand where the terms on the RHS of Eq. 5 are equivalent to those on the RHS of Eq. 6:

$$275 \quad AFFEB_i = \Delta C_i^{land} + \Delta C_i^{ocean} + \Delta C_i^{atmos} + BECCS_i \quad (6)$$

We define the mitigation potential (MP) for a mitigation strategy, j , as the difference between a control AFFEB ($AFFEB_{ctl}$) and the AFFEB resulting from applying the strategy i.e.:

$$MP_j = AFFEB_j - AFFEB_{ctl} \quad (7)$$

which can be broken down into its component parts as:

$$280 \quad MP_j = MP_j^{land} + MP_j^{ocean} + MP_j^{atmos} \\ MP_j = (\Delta C_j^{land} - \Delta C_{ctl}^{land}) + (\Delta C_j^{ocean} - \Delta C_{ctl}^{ocean}) + (\Delta C_j^{atmos} - \Delta C_{ctl}^{atmos}) + BECCS_j \quad (8)$$



2.4.2 Optimisation of the land-based mitigation

Harper et al. (2018) find that the land-use pathways do not provide a clear choice for the preferred mitigation pathway. The key issue is that replacing natural vegetation with bioenergy crops often results in large emissions of soil carbon and the loss of the benefits of maintaining forest carbon stocks. Hence, to optimise the land-based mitigation (LBM), we compare the land-carbon stocks in the IM-1.9 and IM-1.9N scenarios. We then select the optimum land-management option for each grid cell simulated as that which maximises the *AFFEB* by year 2100. That is:

$$AFFEB_{LBM} = \Delta C_{IM1.9}^{atmos} + \Delta C_{IM1.9}^{ocean} + \Delta C_{LBM}^{land} \quad (9)$$

with

$$\Delta C_{LBM}^{land} = \begin{cases} \sum_l^{grid\ cells} \Delta C_{IM1.9}^{land} + BECCS_{IM1.9} & \text{where } \Delta C_{IM1.9N}^{land} < \Delta C_{IM1.9}^{land} + BECCS_{IM1.9} \\ \text{or} & \\ \sum_l^{grid\ cells} \Delta C_{IM1.9N}^{land} & \text{where } \Delta C_{IM1.9N}^{land} > \Delta C_{IM1.9}^{land} + BECCS_{IM1.9} \end{cases} \quad (10)$$

where $\Delta C_{pathway}^{store}$ is the change in carbon between 2015 and 2100 for the ‘store’ (= atmosphere, ocean or land) for the LULUC pathway. We use the ocean and atmosphere contributions from the IM-1.9 simulations as the changes in store size between the IM-1.9 and IM-1.9N simulations are negligible (i.e. <2GtC).

2.4.3 Assumptions about BECCS efficiency

The productivity of the BECCS scheme implemented in JULES is significantly lower than that of other implementations (Harper et al., 2018), reflecting the importance of assumptions about the efficiency of the BECCS process and bioenergy crop yields in determining their ability to contribute to climate mitigation. More specifically, there is (1) large uncertainty in carbon losses from farm to final storage (Harper et al. (2018) assumed a 40% loss compared to 13-52% loss found in other studies); and (2) a large range in potential productivity of second-generation lignocellulosic bioenergy crops, with JULES falling on the low end (JULES in Harper et al. (2018) simulated average yields of ~4.6 tDM ha⁻¹ yr⁻¹ compared to measured median of 11.5 tDM ha⁻¹ yr⁻¹ and simulated average of 15.8 tDM ha⁻¹ yr⁻¹ in IMAGE). As both of these components are assumed to be diagnostics of the simulations, we can modify the contribution of BECCS to the *AFFEB* via a post-processing scaling factor, κ , which represents the efficiency of (1) and (2) with respect to the JULES parameterisation. That is, Eq. 10 becomes:

$$\Delta C_{LBM}^{land} = \begin{cases} \sum_l^{grid\ cells} \Delta C_{IM1.9}^{land} + \kappa BECCS_{IM1.9} & \text{where } \Delta C_{IM1.9N}^{land} < \Delta C_{IM1.9}^{land} + \kappa BECCS_{IM1.9} \\ \text{or} & \\ \sum_l^{grid\ cells} \Delta C_{IM1.9N}^{land} & \text{where } \Delta C_{IM1.9N}^{land} > \Delta C_{IM1.9}^{land} + \kappa BECCS_{IM1.9} \end{cases} \quad (11)$$

Figure 5 presents maps of the scaling factor required for BECCS to be the preferable mitigation option, as opposed to natural land carbon uptake, for each grid cell for warming of 1.5°C or 2°C. There are large factors in the northern temperate and boreal regions, parts of Africa and Australia. As discussed in Harper et al. (2018), this follows from the loss of soil carbon



310 in the tropics and at high northern latitude leading to long recovery or payback times (10-100+ years and >100 years, respectively, Fig. 6(c) in their paper). The payback time is however insignificant when bioenergy crops replace existing agriculture, for example in Europe and eastern North America.

Additionally, we define a threshold efficiency factor, κ^* , which represents the required BECCS efficiency for BECCS to be a preferable mitigation strategy for a given grid-cell, i.e.:

$$\kappa^* = \frac{\Delta C_{IM1.9N}^{land} - \Delta C_{IM1.9}^{land}}{BECCS_{IM1.9}} \quad (12)$$

315 This increased efficiency can be considered to be the additional bioenergy harvest (H) and/or the reduced carbon losses from farm to storage needed to pay back the carbon debt accrued due to land-use change (since carbon removed via BECCS = $H\varepsilon$, where ε is the assumed efficiency factor for farm to storage carbon conservation and H is the simulated biomass harvest). In addition, κ^* implies a new threshold (or break-even) level of BECCS:

$$BECCS^* = \kappa^* * BECCS_{IM1.9} \quad (13)$$

320 In other words, $BECCS^*$ is equivalent to the carbon loss due to the land use change to grow the bioenergy crops. To assess the feasibility of meeting this break-even level of BECCS, we calculate the harvest (H^*) that would be needed if carbon losses are to be minimised, i.e. by increasing ε from 0.6 to 0.87, and assuming in Eq. 13 that:

$$BECCS^* = 0.87 H^* \text{ and } BECCS_{IM1.9} = 0.60 H$$

So:

$$325 \quad H^* = \kappa^* * \frac{0.6}{0.87} * H \quad (14)$$

We discuss this further in Sect. 3.2.

2.5 Model Runs

We undertake control runs and other simulations, with (1) anthropogenic CH₄ mitigation, (2) land-based mitigation or (3) both, stabilising at either 1.5°C or 2.0°C warming without a temperature overshoot, based on the IMAGE SSP2 1.9 (denoted 330 IM-1.9) and baseline (IM-BL) scenarios (Doelman et al., 2018; Riahi et al., 2017) (Sect. 2.3). Table 2 lists the factorial runs, their key features and the prescribed datasets used (for agricultural land and BECCS, anthropogenic emissions and atmospheric concentrations of methane and the non-CO₂ radiative forcing). We denote the anthropogenic CH₄ mitigation scenario as “CH₄”, the land-based mitigation scenario using BECCS as “CCS” and “Natural Land” as focussing on AR. We also undertake coupled runs to see if there are any non-linearities when we combine the methane and land-based mitigation scenarios.

335 For each temperature pathway (1.5°C or 2.0°C) and for the baseline and each mitigation scenario, the set of factorial runs comprises a 136-member ensemble (34 GCMs x 2 ozone damage sensitivities x 2 methanogenesis Q₁₀ temperature



sensitivities). In all model runs, we include the effects of the methane and carbon-climate feedbacks from wetlands and permafrost thaw, which we have shown previously to be significant constraints on the AFFEBs (Comyn-Platt et al., 2018).

As shown in Fig. 1 and discussed in previous sections (Sects 2.2.1 and 2.3), we use a number of prescribed datasets: (a) time series of the annual area of land used for agriculture, including that for BECCS if appropriate; (b) time series of the global annual mean atmospheric concentrations of CH₄ (and N₂O for the radiative forcing calculations of CO₂ and CH₄); (c) time series of the overall radiative forcing by SLCFs and non-CO₂ GHGs (corrected for the radiative forcing of CH₄); and (d) time series of annual anthropogenic methane emissions (used in the post-processing step). We take these from the IMAGE database for the relevant IMAGE SSP2 scenario (baseline or SSP2-1.9). The prescribed datasets used in the different factorial runs are given in Table 2.

The difference in anthropogenic fossil fuel emission budget (AFFEB) between the mitigated pathway and the control simulation gives an estimate of the Mitigation Potential (MP) of the mitigation strategy. The IM-1.9 scenario relies on a combination of BECCS, reduced emissions from deforestation and degradation (REDD), and reforestation of degraded forest areas to achieve a 1.5°C climate target, while IM-BL has limited land-based mitigation via moderate levels of REDD and AR. We develop an additional land-based mitigation scenario (IM-1.9N) where any bioenergy cropland area in IM-1.9 is replaced by natural vegetation (Sect. 2.3). We then derive an optimal land-based mitigation pathway in a post-processing step by selecting the option, (a) BECCS or (b) natural vegetation, which has the more positive impact on the AFFEB in each grid cell (Sect. 2.4.1).

3 Results and Discussion

3.1 Global Perspective

We calculate the anthropogenic fossil fuel emission budget to limit global warming to a particular temperature target as the sum of the changes in the carbon stores of the atmosphere, land (vegetation and soil) and ocean between 2015 and 2100 (Sect. 2.4.1, Eq. 5 and 6). We present in Fig. 6 the median and ensemble member spread of the AFFEB (as box and whiskers), and the individual GCM/ESM contributions to the AFFEBs from the four carbon pools shown (points), for each of the factorial experiments. We find that there is increased uptake of atmospheric CO₂ in the land-based mitigation scenarios, although there is a reduction in land carbon from the land-use changes in these scenarios. In the combined ('coupled') CH₄ and land-based mitigation scenarios, the reduction in the emissions and hence atmospheric concentrations of CH₄ allow increased atmospheric concentrations of CO₂ (Fig. 3(c)-(h)). There is increased uptake of carbon by the land, directly because of the increased atmospheric CO₂ concentration and indirectly through the reduction in O₃ damage, which is greater than the land carbon lost through land-use changes. We also find that there is increased uptake of CO₂ by the oceans for all scenarios. A further co-benefit of reducing the CH₄ emissions and allowing more CO₂ emissions is that the oceanic drawdown of carbon dioxide rises (although there would be implications for ocean acidification). In Fig. 7(a), we compare the AFFEBs for both the 1.5°C and



2°C temperature pathways. We find that the absolute AFFEBs are 200-300 GtC larger for the 2°C target than the 1.5°C target. These budgets are in agreement with other estimates, which include corrections to the historical period (Millar et al., 2017).

370 Figure 7(b) shows the mitigation potential of each strategy, calculated as the change in the AFFEB from the corresponding control simulation, for the two temperature pathways (Sect. 2.4.1, Eq. 7 and 8). Methane mitigation is a highly effective strategy; the AFFEBs are increased by 188-206 GtC and 193-212 GtC for the 1.5°C and 2°C scenarios, respectively, where the range represents the interquartile range from the 136-member ensemble (34 GCMs x 2 Q₁₀ x 2 ozone sensitivities). This AFFEB increase equates to roughly 20-24 years of emissions at current rates for the 1.5°C target. Land-based mitigation
375 strategies also provide significant increases of 51-57 GtC and 56-62 GtC for the 1.5°C and 2°C AFFEB estimates, respectively. This is equivalent to 6-7 years of emissions at current rates. For our BECCS assumptions (see also below), we find that the BECCS contribution is small for the optimised land-based mitigation pathway and that AR are more effective land-based mitigation strategies (Fig. 7(b)).

Furthermore, the CH₄ and land-based mitigation strategies show little interaction and their potential can be summed to
380 give a comparable result to the coupled simulation (coupled vs linear in Fig. 7(a) and (b)). This decoupling is despite the methane emissions from the agricultural sector being influenced by land use choices. We can effectively treat the two mitigation strategies as independent, and their sum approximates the combined potential. Such linearity enables simpler and more direct comparisons.

Despite the substantial differences in the absolute AFFEBs for the 1.5° and 2°C targets, the mitigation potential of the
385 CH₄ and land-based strategies is similar for the two temperature scenarios considered. This similarity suggests that the investment in such strategies is robust to the target temperature; whether the international community aims for the 1.5° or 2°C target, afforestation, reforestation, reduced deforestation and CH₄ mitigation are worthwhile mitigation approaches.

3.2 Sensitivity to BECCS Efficiency

The BECCS parameterisation used here makes BECCS less effective compared to those in other studies (van Vuuren et al., 2018). Globally, our simulations imply a removal of 27-30 GtC from the active carbon-cycle atmosphere via BECCS in
390 the original IM-1.9 simulation, which is reduced to ~7-12 GtC after we optimise the land-use scenario. These removal rates are significantly lower than other estimates based on the same land-use scenarios: 73 GtC in a similar dynamic global vegetation model (LPJ-GUESS) and 130 GtC in IMAGE (Harper et al., 2018). We find that doubling the carbon captured with BECCS in our simulations (Sect. 2.4.3, $\kappa=2$) has a relatively small impact on the total mitigation potential in the optimised
395 scenario (Fig. 8(a)). This low sensitivity is because the increased carbon removed by BECCS often accompanies a comparable decrease in the carbon uptake from the “natural” vegetation that it replaces. It is only when setting the BECCS carbon sequestration at 3-5 times its original value that there is a notable increase of the global AFFEB. Further, as shown in Fig. 8(b), there is reduction in soil carbon in specific regions (e.g. Northern temperate and boreal regions), which makes BECCS less effective for carbon sequestration than natural land management options (or there is a long payback time as discussed in Harper
400 et al. (2018)).



Increased carbon removal with BECCS could be realised through either (1) minimizing the loss of carbon from farm to final storage (ε in Sect. 2.4.3), or (2) maximizing the productivity of the bioenergy crop. Our IMOGEN-JULES simulations assume a 40% carbon loss from farm to final storage, although other studies have assumed this to be as low as 13% (Harper et al., 2018). The bioenergy crop yields in JULES (Fig. 8(c)) are lower than the median yield of Miscanthus (11.5 tons of dry matter (ton DM) $\text{ha}^{-1} \text{yr}^{-1}$), measured from 990 mostly European plots (Li et al., 2018), and are about half the productivity of those in the IMAGE simulations. We calculate for each IMOGEN grid cell the increase in carbon removed via BECCS and the associated increase in bioenergy crop yields (H^* in Sect. 2.4.3) required for BECCS to be the preferred mitigation option (Fig. 8(d)), rather than natural land carbon uptake, and assuming minimal amounts of carbon are lost during the BECCS lifecycle (13% carbon loss). In many places, the required yield increases from <10 to $10\text{-}20$ ton DM $\text{ha}^{-1} \text{yr}^{-1}$ are achievable, but yields of > 30 ton DM $\text{ha}^{-1} \text{yr}^{-1}$ would be more difficult to realise (Li et al., 2018).

We conclude that our uncorrected simulations are a lower estimate for the potential of carbon removal via BECCS. We provide a more optimistic estimate of the BECCS potential using $\kappa = 3$, which results from doubling the JULES yields and increasing the efficiency ε from 0.6 to 0.87 (i.e., $\kappa \sim 2 \times 0.87 / 0.6$). We now find the global land-based mitigation potential to be 56-62 GtC, as shown in Fig. 7(c) and (d). We use $\kappa = 3$ in the subsequent analysis of regional mitigation options and of BECCS water requirements.

3.3 Regional Analysis

We consider the sub-continental implications of CH_4 and land-based mitigation options, using the 26 regions of the IMAGE model (Stehfest et al., 2014). Figure 9 shows the contributions of the three mitigation options - CH_4 , carbon uptake through AR and BECCS - to the AFFEBs for each IMAGE region and for the temperature pathway stabilising at 1.5°C .

We estimate the regional land-based mitigation as the change in the land-carbon stores plus the carbon removal via BECCS for each IMAGE region in the IMOGEN-JULES model output. In this accounting, the region where the bioenergy crops are grown is credited with the carbon removal via BECCS. We assume a three-fold increase in carbon removal via BECCS compared to our default simulations ($\kappa=3$) to highlight regions where BECCS is potentially viable. Figure 10 shows the sensitivity of the global AFFEBs and Mitigation Potential for $\kappa = 1, 2$ and 3 for 1.5°C of warming (Supplementary Information, Figure SI.2 is the corresponding figure for 2°C of warming). For CH_4 , we derive the regional contribution to the changes in the global atmospheric CH_4 concentration, and therefore the CH_4 mitigation potential, using regional fractions of the global difference in anthropogenic CH_4 emissions (2020-2100) between the IMAGE SSP2-Baseline and SSP2-1.9 scenarios (van Vuuren et al., 2017) (Table 3). These two CH_4 scenarios are consistent with the CH_4 concentration pathways considered in the CH_4 factorial simulations (Sect. 2.3).

CH_4 mitigation generally has a larger impact on emission budget reductions, is an effective mitigation strategy for all regions, and especially the major methane emitting regions: India, S. Africa, USA, China and Australasia. Figure 4 presented time series of the anthropogenic methane emissions for selected IMAGE region from 2000 to 2100 (and Supplementary Information, Figure SI.1 presents emission time series for all IMAGE regions). The mitigation of CH_4 emissions from fossil-



435 fuel production, distribution and use for energy is the largest contributor for India, S. Africa, USA, China and Australasia. The emissions from agriculture-cattle (for India, USA and China) and rice production (China and other Asian regions) make smaller contributions.

The impact of the land-based mitigation options links strongly to the managed land-use and land-use change (LULUC). Table 1 lists the maximum area of BECCS deployed in each IMAGE region and the main differences in land use between the IM-1.9 and IM-1.9N scenarios. Figure 11 presents time series of the land areas calculated for trees and prescribed for
440 agriculture (including bioenergy crops) and bioenergy crops for the IM-1.9 and IM-1.9N scenarios for the Russia and Brazil IMAGE regions, each as a difference to the baseline scenario (IM-BL) (Supplementary Information, Figure SI.3 is equivalent to Fig. 11 for all the IMAGE regions). The West Africa region shows the largest natural land carbon uptake (WAF in Fig. 10). Here, there is conversion of crop and pasture to forest, with little land used for bioenergy crops for BECCS. For Brazil (Fig. 11(a)) and the rest of South America, both bioenergy crops and forest expand at the expense of agricultural land. For many
445 other regions, notably Canada, Russia, W. & C. Europe, China, Oceania, there is less carbon uptake from the ‘land’ in the optimised mitigation scenario, even though the overall carbon uptake has increased. For Canada and Russia, this results from the loss of forest in the BECCS land use scenario (see Fig. 11(b) and Supplementary Information, Figure SI.3). The carbon uptake by BECCS increases as κ increases from 1 to 3 because there are more grid cells where ‘BECCS’ is the preferred mitigation option in the optimisation process. As κ only affects the ‘BECCS’ term (Sect. 2.4.3, Eq. 11), the increased carbon
450 removed by BECCS is often accompanied by a decrease in the carbon uptake from the “natural” vegetation that it replaces. This can be seen more clearly in Fig. 10 (and Supplementary Information, Figure SI.2 for 2°C warming). The version of JULES used in this study currently lacks a fire regime. There will be risks to long-term storage of carbon stored in vegetation in regions with significant areas of fire-dominated vegetation cover (e.g. savannah in Brazil and Africa). Further, this version of JULES does not include a nitrogen cycle, which has been implemented in more recent versions of the model. This will enable the
455 impact of changes in land use and agriculture on N₂O emissions to be integrated into the assessments.

There is relatively little difference in the allowable carbon emission budgets between 2015 and 2100 for the two temperature scenarios considered (Supplementary Information, Figure SI.4 for the contributions at 2°C of warming).

3.4 Water Resources

Smith et al. (2016) estimate the global water requirements for different negative emission technologies, including BECCS.
460 We also derive the water requirements from the carbon uptake by BECCS for our optimised land-based mitigation scenarios. We set $\kappa = 3$ and assume (a) a marginal increase in water use of 80 m³ (tC eq)⁻¹ yr⁻¹ when replacing the average short vegetation (i.e., C3/C4 grasses in JULES) by a biomass energy crop (Smith et al., 2016); and (b) 450 m³ (tC eq)⁻¹ yr⁻¹ for the CCS component (Smith et al., 2016).

Following Postel et al. (1996), we derive the accessible runoff, assuming that only 5% of the total runoff is accessible for
465 the Brazil, Russia and Canada IMAGE regions and 40% elsewhere. Our present-day estimates of the global annual runoff



(43,000-44,200 km³ yr⁻¹) and the accessible runoff for human use (11,400-11,720 km³ yr⁻¹) (see Fig. 12) are both in agreement with the values given in Postel et al. (1996), i.e., total and accessible runoffs of 40,700 and 12,500 km³ yr⁻¹, respectively.

We take the water requirements for agricultural irrigation (Rost et al., 2008) and for other human activities (Bijl et al., 2016) (Table 4), as the total water withdrawal for each IMAGE region from the IMAGE-SSP2-RCP2.6 scenarios. We note
470 that the irrigation water withdrawal, derived using the coupled IMAGE-LPJmL models, are low compared to other estimates in the literature.

Figure 13 compares the accessible water with the water demand for BECCS and other human activities for the eight regions, which produce a substantial amount of BECCS: Canada, USA, Brazil, Europe, Russia, China, Southern Africa and Oceania. Our estimates represent a maximum possible water usage for BECCS as (i) the SSP2 scenario used already accounts
475 for the lower power generation efficiencies and hence higher water requirements in switching from fossil fuels to bioenergy crops (which could be up to 20-25%) and (ii) the figure used for the CCS component does not allow for future technological improvements in water use. For example, Fajardy and Mac Dowell (2017) indicate a 30-fold reduction in water use when changing from a once-through to a recirculating cooling tower. Our results are less severe than other studies considering BECCS water requirements (Séférian et al., 2018; Yamagata et al., 2018), because the carbon removed by BECCS in this study
480 (30 GtC) is already limited to regions where it is more beneficial to the AFFEB than forest-based mitigation options. Nevertheless, the additional water demand for BECCS would make it impractical in half of the regions substantially invested in BECCS: Oceania, Rest of South Africa and China (2060).

4 Conclusions

Our paper brings together previous studies that looked separately into the potential of methane mitigation (Collins et al.,
485 2018) and land-management options (especially forest conservation and BECCS) (Harper et al., 2018), into a single unified framework. Uniquely, this allows us to compare these options at local and regional scales. We utilise the detailed JULES land-surface model, which includes the temperature sensitivity of methanogenesis (Comyn-Platt et al., 2018) and the effect of methane emissions on land carbon storage via ozone impacts on vegetation (Sitch et al., 2007), and also span the range of climate model projections using the IMOGEN ESM-emulator. For each temperature pathway and each of the three mitigation
490 options, the set of factorial runs comprises a 136-member ensemble (34 GCMs x 2 ozone damage sensitivities x 2 methanogenesis Q₁₀ temperature sensitivities).

This analysis quantifies the regional differences in potential CH₄ and land-based strategies to aid mitigation of climate change. Our findings are presented within a full probabilistic framework, capturing uncertainty in climate projections across the CMIP5 ensemble, as well as process uncertainties associated with the strength of natural CH₄ climate feedbacks from
495 wetlands and ozone vegetation damage. We acknowledge that land surface models still require refinement, alongside improved characterisation of the assumptions inherent in the socio-economic pathways and IAM modelling. Further, we do not allow



for the reduced emissions from fossil fuel combustion due to the bioenergy crop being grown, as this would require energy sector modelling that is beyond the scope of this study.

We quantify a strong sensitivity to the assumed productivity of bioenergy crops and the efficiency of the BECCS process. In consequence, our results for land-based mitigation strategies are nuanced, with considerable regional variations. For boreal forest regions there is a preference for avoided deforestation, whereas in tropical forest regions both AR and avoided deforestation offer significant potential. From a carbon sequestration perspective, growing bioenergy crops for BECCS is only preferable where it replaces existing agricultural land. BECCS has particular potential if productivities and power production efficiencies are towards the upper limit of expected photosynthetic capability, whilst noting the strong water demand of such crops requires consideration in the context of a growing population.

Our overarching finding is however robust to these uncertainties. We conclude that CH₄ mitigation can be a highly effective route to meeting the Paris Agreement targets, and could offset up to 188-212 GtC of anthropogenic CO₂ emissions. It is effective globally and especially so for the major CH₄-emitting regions of India, USA and China.

Code and Data Availability

The JULES source code used in this work is available from the JULES code repository (https://code.metoffice.gov.uk/trac/jules/browser/main/branches/dev/annaharper/r7971_vn4.8_IP5_DEGREES_CCS, at JULES revision 14477, user account required). The rose suites used for the specific factorial runs are: u-as624, u-at010, u-at011, u-at013, u-av005, u-av007, u-av008, u-av009, u-ax327, u-ax332, u-ax455, u-ax456, u-ax521, u-ax523, u-ax524, u-ax525, u-bh009, u-bh023, u-bh046, u-bh081, u-bh084, u-bh098, u-bh103 and u-bh105. These can be found at <https://code.metoffice.gov.uk/trac/roses-u/> (user account required).

All code, data and parameterisations are available on request to the corresponding author.

Author Contributions

G.H., C.H., E.C-P., A.H., P.C., T.P., J.H., W.C., J.L. and S.C. designed the IMOGEN runs. All authors contributed to the interpretation of the results and to the writing of or review of the paper. C.H. provided IMOGEN parameters calibrated against the CMIP5 database, and E.C-P and C.H. led the development of the inverse IMOGEN model version. The following specific contributions were also made: (a) E.B., S.C. and N.G.: code and expertise on permafrost, soil carbon and wetland methane modelling, respectively; (b) A.H. and T.P.: land use change data; (c) W.C. and C.W.: ozone ancillary data; (d) D.P.vV. and J.C.D.: IMAGE scenario data on land use, anthropogenic methane emissions and water consumption and withdrawals, and (e) S.S.: expertise on the ozone damage effects.



525 Competing interests

The authors declare no competing interests.

Acknowledgements

The work was undertaken as part of the UK Natural Environment Research Council's programme "Understanding the Pathways to and Impacts of a 1.5°C Rise in Global Temperature" through grants NE/P015050/1 CLIFFTOP (G.H., E.C-P, S.C.), NE/P014909/1, MOC1.5 (W.C., C.W., J.L., C.H., P.C., S.S.) and NE/P014941/1 CLUES (P.C., A.H., T.P., J.H.). We also acknowledge the support for: (a) G.H and E.C.P by NERC NE/N015746/1 The Global Methane Budget, MOYA; (b) A.H. through her EPSRC Fellowship "Negative Emissions and the Food-Energy-Water Nexus" (EP/N030141/1); (c) A.H. by NERC NE/P019951/1 FAB GGR, (d) W.C. from the Research Council of Norway, project no. 235548; (e) C.H. from CEH National Capability Funding; (f) E.B. and N.G. from the Joint UK BEIS/Defra Met Office Hadley Centre Climate Programme (GA01101); (g) E.B., D.P.vV. and J.C.D. from CRESCENDO (EU project 641816). All authors acknowledge the CMIP5 database, and its outputs from Earth System Models developed by climate research centres across the world. We also acknowledge Lars Kutzbach and David Holl, who kindly provided the methane emission data for the Samoylov Island field site.

References

- 540 Anderson, K., and Peters, G.: The trouble with negative emissions, *Science*, 354, 182, <https://doi.org/10.1126/science.aah4567>, 2016.
- Best, M., Pryor, M., Clark, D., Rooney, G., Essery, R., Ménard, C., Edwards, J., Hendry, M., Porson, A., and Gedney, N.: The Joint UK Land Environment Simulator (JULES), model description—Part 1: energy and water fluxes, *Geoscientific Model Development*, 4, 677-699, <https://doi.org/10.5194/gmd-4-677-2011>, 2011.
- 545 Bijl, D. L., Bogaart, P. W., Kram, T., de Vries, B. J. M., and van Vuuren, D. P.: Long-term water demand for electricity, industry and households, *Environmental Science & Policy*, 55, 75-86, <https://doi.org/10.1016/j.envsci.2015.09.005>, 2016.
- Burke, E. J., Chadburn, S. E., and Ekici, A.: A vertical representation of soil carbon in the JULES land surface scheme (vn4. 3_permafrost) with a focus on permafrost regions, *Geoscientific Model Development*, 10, 959, <https://doi.org/10.5194/gmd-10-959-2017>, 2017a.
- Burke, E. J., Ekici, A., Huang, Y., Chadburn, S. E., Huntingford, C., Ciais, P., Friedlingstein, P., Peng, S., and Krinner, G.: Quantifying uncertainties of permafrost carbon-climate feedbacks, *Biogeosciences*, 14, 3051-3066, <https://doi.org/10.5194/bg-14-3051-2017>, 2017b.
- 550 Chadburn, S., Burke, E., Essery, R., Boike, J., Langer, M., Heikenfeld, M., Cox, P., and Friedlingstein, P.: An improved representation of physical permafrost dynamics in the JULES land-surface model, *Geoscientific Model Development*, 8, 1493-1508, <https://doi.org/10.5194/gmd-8-1493-2015>, 2015.



- 555 Chadburn, S., Fan, Y., Burke, E., Aalto, T., Aurela, M., Biasi, C., Boike, J., Comyn-Platt, E., Dolman, H., Friborg, T., Gao, Y., Gedney, N., Hayman, G., Holl, D., Hugelius, G., Kutzbach, L., Lee, H., Lohila, A., Parmentier, F.-J., Sachs, T., Shurpali, N., Westermann, S., Göckede, M., and Baldocchi, D.: Modeled microbial dynamics explain the apparent temperature-sensitivity of wetland methane emissions, *Global Biogeochemical Cycles*, Submitted, 2020.
- 560 Clark, D., Mercado, L., Sitch, S., Jones, C., Gedney, N., Best, M., Pryor, M., Rooney, G., Essery, R., Blyth, E., Boucher, O., Harding, R., Huntingford, C., and Cox, P.: The Joint UK Land Environment Simulator (JULES), model description - Part 2: Carbon fluxes and vegetation dynamics, *Geoscientific Model Development*, 4, 701-722, <https://doi.org/10.5194/gmd-4-701-2011>, 2011.
- Collins, W. J., Webber, C. P., Cox, P. M., Huntingford, C., Lowe, J., Sitch, S., Chadburn, S. E., Comyn-Platt, E., Harper, A. B., Hayman, G., and Powell, T.: Increased importance of methane reduction for a 1.5 degree target, *Environmental Research Letters*, 13, 054003, <https://doi.org/10.1088/1748-9326/aab89c>, 2018.
- 565 Comyn-Platt, E., Hayman, G., Huntingford, C., Chadburn, S. E., Burke, E. J., Harper, A. B., Collins, W. J., Webber, C. P., Powell, T., Cox, P. M., Gedney, N., and Sitch, S.: Carbon budgets for 1.5 and 2 °C targets lowered by natural wetland and permafrost feedbacks, *Nature Geoscience*, 11, 568-573, <https://doi.org/10.1038/s41561-018-0174-9>, 2018.
- 570 Cubasch, U., Meehl, G. A., Boer, G. J., Stouffer, R. J., Dix, M., Noda, A., Senior, C. A., Raper, S., and Yap, K. S.: Projections of Future Climate Change In: *Climate Change 2001: The Scientific Basis. Contribution of Working Group I to the Third Assessment Report of the Intergovernmental Panel on Climate Change* [Houghton, J.T., Y. Ding, D.J. Griggs, M. Noguer, P.J. van der Linden, X. Dai, K. Maskell, and C.A. Johnson (eds.)]. Cambridge University Press, Cambridge, United Kingdom and New York, NY, USA, 881pp., Available from: <https://www.ipcc.ch/report/ar3/wg1/> (accessed November 2019). 2001.
- Daioglou, V., Doelman, J. C., Wicke, B., Faaij, A., and van Vuuren, D. P.: Integrated assessment of biomass supply and demand in climate change mitigation scenarios, *Global Environmental Change*, 54, 88-101, <https://doi.org/10.1016/j.gloenvcha.2018.11.012>, 2019.
- 575 Doelman, J. C., Stehfest, E., Tabeau, A., van Meijl, H., Lassaletta, L., Gernaat, D. E. H. J., Hermans, K., Harmsen, M., Daioglou, V., Biemans, H., van der Sluis, S., and van Vuuren, D. P.: Exploring SSP land-use dynamics using the IMAGE model: Regional and gridded scenarios of land-use change and land-based climate change mitigation, *Global Environmental Change*, 48, 119-135, <https://doi.org/10.1016/j.gloenvcha.2017.11.014>, 2018.
- Etminan, M., G. Myhre, E. J. Highwood, and Shine, K. P.: Radiative forcing of carbon dioxide, methane, and nitrous oxide: A significant revision of the methane radiative forcing, *Geophysical Research Letters*, 43, <https://doi.org/10.1002/2016GL071930>, 2016.
- 580 Fajardy, M., and Mac Dowell, N.: Can BECCS deliver sustainable and resource efficient negative emissions?, *Energy & Environmental Science*, 10, 1389-1426, <https://doi.org/10.1039/C7EE00465F>, 2017.
- 585 Fuss, S., Lamb, W. F., Callaghan, M. W., Hilaire, J., Creutzig, F., Amann, T., Beringer, T., Garcia, W. d. O., Hartmann, J., Khanna, T., Luderer, G., Nemet, G. F., Rogelj, J., Smith, P., Vicente, J. L. V., Wilcox, J., M. del Mar Zamora, D., and Minx, J. C.: Negative emissions—Part 2: Costs, potentials and side effects, *Environmental Research Letters*, 13, 063002, <https://doi.org/10.1088/1748-9326/aabf9f>, 2018.
- Gasser, T., Kechiar, M., Ciais, P., Burke, E. J., Kleinen, T., Zhu, D., Huang, Y., Ekici, A., and Obersteiner, M.: Path-dependent reductions in CO₂ emission budgets caused by permafrost carbon release, *Nature Geoscience*, <https://doi.org/10.1038/s41561-018-0227-0>, 2018.



- Gedney, N., Huntingford, C., Comyn-Platt, E., and Wiltshire, A.: Significant feedbacks of wetland methane release on climate change and the causes of their uncertainty, *Environmental Research Letters*, 14, 084027, <https://doi.org/10.1088/1748-9326/ab2726>, 2019.
- 590 Gernaat, D. E. H. J., Calvin, K., Lucas, P. L., Luderer, G., Otto, S. A. C., Rao, S., Strefler, J., and van Vuuren, D. P.: Understanding the contribution of non-carbon dioxide gases in deep mitigation scenarios, *Global Environmental Change*, 33, 142-153, <https://doi.org/10.1016/j.gloenvcha.2015.04.010>, 2015.
- Harper, A. B., Cox, P. M., Friedlingstein, P., Wiltshire, A. J., Jones, C. D., Sitch, S., Mercado, L. M., Groenendijk, M., Robertson, E., Kattge, J., Bönisch, G., Atkin, O. K., Bahn, M., Cornelissen, J., Niinemets, Ü., Onipchenko, V., Peñuelas, J., Poorter, L., Reich, P. B.,
595 Soudzilovskaia, N. A., and Bodegom, P. V.: Improved representation of plant functional types and physiology in the Joint UK Land Environment Simulator (JULES v4.2) using plant trait information, *Geoscientific Model Development*, 9, 2415-2440, 10.5194/gmd-9-2415-2016, 2016.
- Harper, A. B., Powell, T., Cox, P. M., House, J., Huntingford, C., Lenton, T. M., Sitch, S., Burke, E., Chadburn, S. E., Collins, W. J., Comyn-Platt, E., Daioglou, V., Doelman, J. C., Hayman, G., Robertson, E., van Vuuren, D., Wiltshire, A., Webber, C. P., Bastos, A., Boysen,
600 L., Ciais, P., Devaraju, N., Jain, A. K., Krause, A., Poulter, B., and Shu, S.: Land-use emissions play a critical role in land-based mitigation for Paris climate targets, *Nature Communications*, 9, 2938, <https://doi.org/10.1038/s41467-018-05340-z>, 2018.
- Heck, V., Gerten, D., Lucht, W., and Popp, A.: Biomass-based negative emissions difficult to reconcile with planetary boundaries, *Nature Climate Change*, 8, 151-155, <https://doi.org/10.1038/s41558-017-0064-y>, 2018.
- Hoogwijk, M., Faaij, A., de Vries, B., and Turkenburg, W.: Exploration of regional and global cost–supply curves of biomass energy from short-rotation crops at abandoned cropland and rest land under four IPCC SRES land-use scenarios, *Biomass and Bioenergy*, 33, 26-
605 43, <https://doi.org/10.1016/j.biombioe.2008.04.005>, 2009.
- Huntingford, C., Booth, B. B. B., Sitch, S., Gedney, N., Lowe, J. A., Liddicoat, S. K., Mercado, L. M., Best, M. J., Weedon, G. P., Fisher, R. A., Lomas, M. R., Good, P., Zelazowski, P., Everitt, A. C., Spessa, A. C., and Jones, C. D.: IMOGEN: an intermediate complexity model to evaluate terrestrial impacts of a changing climate, *Geoscientific Model Development*, 3, 679-687,
610 <https://doi.org/10.5194/gmd-3-679-2010>, 2010.
- Huntingford, C., Yang, H., Harper, A., Cox, P. M., Gedney, N., Burke, E. J., Lowe, J. A., Hayman, G., Collins, W. J., Smith, S. M., and Comyn-Platt, E.: Flexible parameter-sparse global temperature time profiles that stabilise at 1.5 and 2.0 degrees C, *Earth System Dynamics*, 8, 617-626, <https://doi.org/10.5194/esd-8-617-2017>, 2017.
- IPCC: Global Warming of 1.5 °C, IPCC special report on the impacts of global warming of 1.5 °C above pre-industrial levels and related global greenhouse gas emission pathways, in the context of strengthening the global response to the threat of climate change, sustainable development, and efforts to eradicate poverty, Available from: <http://www.ipcc.ch/report/sr15/> (accessed November 2019). 2018.
- 615 IPCC: Climate Change and Land, IPCC Special Report on climate change, desertification, land degradation, sustainable land management, food security, and greenhouse gas fluxes in terrestrial ecosystems, Available from: <https://www.ipcc.ch/report/srccl/> (accessed November 2019). 2019.



- 620 Jones, C., Hughes, J., Bellouin, N., Hardiman, S., Jones, G., Knight, J., Liddicoat, S., O'Connor, F., Andres, R. J., and Bell, C.: The HadGEM2-ES implementation of CMIP5 centennial simulations, *Geoscientific Model Development*, 4, 543, <https://doi.org/10.5194/gmd-4-543-2011>, 2011.
- Klein Goldewijk, K., Beusen, A., Van Drecht, G., and De Vos, M.: The HYDE 3.1 spatially explicit database of human-induced global land-use change over the past 12,000 years, *Global Ecology and Biogeography*, 20, 73-86, <https://doi.org/10.1111/j.1466-8238.2010.00587.x>, 2011.
- 625 Krause, A., Pugh, T. A. M., Bayer, A. D., Doelman, J. C., Humpenöder, F., Anthoni, P., Olin, S., Bodirsky, B. L., Popp, A., Stehfest, E., and Arneith, A.: Global consequences of afforestation and bioenergy cultivation on ecosystem service indicators, *Biogeosciences*, 14, 4829-4850, <https://doi.org/10.5194/bg-14-4829-2017>, 2017.
- Le Quéré, C., Andrew, R. M., Friedlingstein, P., Sitch, S., Hauck, J., Pongratz, J., Pickers, P. A., Korsbakken, J. I., Peters, G. P., Canadell, J. G., Arneith, A., Arora, V. K., Barbero, L., Bastos, A., Bopp, L., Chevallier, F., Chini, L. P., Ciais, P., Doney, S. C., Gkritzalis, T., Goll, D. S., Harris, I., Haverd, V., Hoffman, F. M., Hoppema, M., Houghton, R. A., Hurtt, G., Ilyina, T., Jain, A. K., Johannessen, T., Jones, C. D., Kato, E., Keeling, R. F., Goldewijk, K. K., Landschützer, P., Lefèvre, N., Lienert, S., Liu, Z., Lombardozzi, D., Metzl, N., Munro, D. R., Nabel, J. E. M. S., Nakaoka, S. I., Neill, C., Olsen, A., Ono, T., Patra, P., Peregón, A., Peters, W., Peylin, P., Pfeil, B., Pierrot, D., Poulter, B., Rehder, G., Resplandy, L., Robertson, E., Rocher, M., Rödenbeck, C., Schuster, U., Schwinger, J., Séférian, R., Skjelvan, I., Steinhoff, T., Sutton, A., Tans, P. P., Tian, H., Tilbrook, B., Tubiello, F. N., van der Laan-Luijkx, I. T., van der Werf, G. R., Viovy, N., Walker, A. P., Wiltshire, A. J., Wright, R., Zaehle, S., and Zheng, B.: Global Carbon Budget 2018, *Earth Syst. Sci. Data*, 10, 2141-2194, <https://doi.org/10.5194/essd-10-2141-2018>, 2018.
- 630 Li, W., Ciais, P., Makowski, D., and Peng, S.: A global yield dataset for major lignocellulosic bioenergy crops based on field measurements, *Scientific Data*, 5, 180169, <https://doi.org/10.1038/sdata.2018.169>, 2018.
- 640 McNorton, J., Gloor, E., Wilson, C., Hayman, G. D., Gedney, N., Comyn-Platt, E., Marthews, T., Parker, R. J., Boesch, H., and Chipperfield, M. P.: Role of regional wetland emissions in atmospheric methane variability, *Geophysical Research Letters*, 43, 11,433-411,444, 10.1002/2016gl070649, 2016.
- Melton, J., Wania, R., Hodson, E., Poulter, B., Ringeval, B., Spahni, R., Bohn, T., Avis, C., Beerling, D., Chen, G., Eliseev, A., Denisov, S., Hopcroft, P., Lettenmaier, D., Riley, W., Singarayer, J., Subin, Z., Tian, H., Zurcher, S., Brovkin, V., van Bodegom, P., Kleinen, T., Yu, Z., and Kaplan, J.: Present state of global wetland extent and wetland methane modelling: conclusions from a model inter-comparison project (WETCHIMP), *Biogeosciences*, 10, 753-788, <https://doi.org/10.5194/bg-10-753-2013>, 2013.
- 645 Millar, R. J., Fuglestedt, J. S., Friedlingstein, P., Rogelj, J., Grubb, M. J., Matthews, H. D., Skeie, R. B., Forster, P. M., Frame, D. J., and Allen, M. R.: Emission budgets and pathways consistent with limiting warming to 1.5 °C, *Nature Geoscience*, 10, 741, <https://doi.org/10.1038/ngeo3031>, 2017.
- 650 Myhre, G., Shindell, D., Bréon, F.-M., Collins, W., Fuglestedt, J. H., J., Koch, D., Lamarque, J.-F., Lee, D., Mendoza, B., Nakajima, T., Robock, A., Stephens, G., Takemura, T., and Zhang, H.: Anthropogenic and Natural Radiative Forcing. In: *Climate Change 2013: The Physical Science Basis. Contribution of Working Group I to the Fifth Assessment Report of the Intergovernmental Panel on Climate Change*, in: IPCC, 2013: *Climate Change 2013*, edited by: Stocker, T. F., Qin, G.-K., Plattner, M., Tignor, S.K., Allen, J., Boschung,



- 655 A. Nauels, Y. Xia, V. Bex and P.M. Midgley (eds.), Cambridge University Press, Cambridge, United Kingdom and New York, NY, USA., 2013.
- O'Neill, B. C., Kriegler, E., Ebi, K. L., Kemp-Benedict, E., Riahi, K., Rothman, D. S., van Ruijven, B. J., van Vuuren, D. P., Birkmann, J., Kok, K., Levy, M., and Solecki, W.: The roads ahead: Narratives for shared socioeconomic pathways describing world futures in the 21st century, *Global Environmental Change*, 42, 169-180, <https://doi.org/10.1016/j.gloenvcha.2015.01.004>, 2017.
- 660 Oliver, R. J., Mercado, L. M., Sitch, S., Simpson, D., Medlyn, B. E., Lin, Y. S., and Folberth, G. A.: Large but decreasing effect of ozone on the European carbon sink, *Biogeosciences*, 15, 4245-4269, <https://doi.org/10.5194/bg-15-4245-2018>, 2018.
- Postel, S. L., Daily, G. C., and Ehrlich, P. R.: Human Appropriation of Renewable Fresh Water, *Science*, 271, 785, <https://doi.org/10.1126/science.271.5250.785>, 1996.
- Riahi, K., van Vuuren, D. P., Kriegler, E., Edmonds, J., O'Neill, B. C., Fujimori, S., Bauer, N., Calvin, K., Dellink, R., Fricko, O., Lutz, W., Popp, A., Cuaresma, J. C., Kc, S., Leimbach, M., Jiang, L., Kram, T., Rao, S., Emmerling, J., Ebi, K., Hasegawa, T., Havlik, P., 665 Humpenöder, F., Da Silva, L. A., Smith, S., Stehfest, E., Bosetti, V., Eom, J., Gernaat, D., Masui, T., Rogelj, J., Strefler, J., Drouet, L., Krey, V., Luderer, G., Harmsen, M., Takahashi, K., Baumstark, L., Doelman, J. C., Kainuma, M., Klimont, Z., Marangoni, G., Lotze-Campen, H., Obersteiner, M., Tabeau, A., and Tavoni, M.: The Shared Socioeconomic Pathways and their energy, land use, and greenhouse gas emissions implications: An overview, *Global Environmental Change*, 42, 153-168, <https://doi.org/10.1016/j.gloenvcha.2016.05.009>, 2017.
- 670 Rogelj, J., Popp, A., Calvin, K. V., Luderer, G., Emmerling, J., Gernaat, D., Fujimori, S., Strefler, J., Hasegawa, T., Marangoni, G., Krey, V., Kriegler, E., Riahi, K., van Vuuren, D. P., Doelman, J. C., Drouet, L., Edmonds, J., Fricko, O., Harmsen, M., Havlík, P., Humpenöder, F., Stehfest, E., and Tavoni, M.: Scenarios towards limiting global mean temperature increase below 1.5 °C, *Nature Climate Change*, 8, 325-332, <https://doi.org/10.1038/s41558-018-0091-3>, 2018.
- 675 Rost, S., Gerten, D., Bondeau, A., Lucht, W., Rohwer, J., and Schaphoff, S.: Agricultural green and blue water consumption and its influence on the global water system, *Water Resources Research*, 44, <https://doi.org/10.1029/2007WR006331>, 2008.
- Saunio, M., Bousquet, P., Poulter, B., Peregon, A., Ciais, P., Canadell, J. G., Dlugokencky, E. J., Etiope, G., Bastviken, D., Houweling, S., Janssens-Maenhout, G., Tubiello, F. N., Castaldi, S., Jackson, R. B., Alexe, M., Arora, V. K., Beerling, D. J., Bergamaschi, P., Blake, D. R., Brailsford, G., Brovkin, V., Bruhwiler, L., Crevoisier, C., Crill, P., Covey, K., Curry, C., Frankenberg, C., Gedney, N., Höglund-Isaksson, L., Ishizawa, M., Ito, A., Joos, F., Kim, H. S., Kleinen, T., Krummel, P., Lamarque, J. F., Langenfelds, R., Locatelli, R., 680 Machida, T., Maksyutov, S., McDonald, K. C., Marshall, J., Melton, J. R., Morino, I., Naik, V., O'Doherty, S., Parmentier, F. J. W., Patra, P. K., Peng, C., Peng, S., Peters, G. P., Pison, I., Prigent, C., Prinn, R., Ramonet, M., Riley, W. J., Saito, M., Santini, M., Schroeder, R., Simpson, I. J., Spahni, R., Steele, P., Takizawa, A., Thornton, B. F., Tian, H., Tohjima, Y., Viovy, N., Voulgarakis, A., van Weele, M., van der Werf, G. R., Weiss, R., Wiedinmyer, C., Wilton, D. J., Wiltshire, A., Worthy, D., Wunch, D., Xu, X., Yoshida, Y., Zhang, B., Zhang, Z., and Zhu, Q.: The global methane budget 2000–2012, *Earth Syst. Sci. Data*, 8, 697-751, 10.5194/essd-8-697-2016, 2016.
- 685 Saunio, M., Stavert, A. R., Poulter, B., Bousquet, P., Canadell, J. G., Jackson, R. B., Raymond, P. A., Dlugokencky, E. J., Houweling, S., Patra, P. K., Ciais, P., Arora, V. K., Bastviken, D., Bergamaschi, P., Blake, D. R., Brailsford, G., Bruhwiler, L., Carlson, K. M., Carrol,



- 690 M., Castaldi, S., Chandra, N., Crevoisier, C., Crill, P. M., Covey, K., Curry, C. L., Etiopie, G., Frankenberg, C., Gedney, N., Hegglin,
M. I., Höglund-Isakson, L., Hugelius, G., Ishizawa, M., Ito, A., Janssens-Maenhout, G., Jensen, K. M., Joos, F., Kleinen, T., Krummel,
P. B., Langenfelds, R. L., Laruelle, G. G., Liu, L., Machida, T., Maksyutov, S., McDonald, K. C., McNorton, J., Miller, P. A., Melton,
J. R., Morino, I., Müller, J., Murgia-Flores, F., Naik, V., Niwa, Y., Noce, S., O'Doherty, S., Parker, R. J., Peng, C., Peng, S., Peters, G.
P., Prigent, C., Prinn, R., Ramonet, M., Regnier, P., Riley, W. J., Rosentreter, J. A., Segers, A., Simpson, I. J., Shi, H., Smith, S. J.,
Steele, P. L., Thornton, B. F., Tian, H., Tohjima, Y., Tubiello, F. N., Tsuruta, A., Viovy, N., Voulgarakis, A., Weber, T. S., van Weele,
M., van der Werf, G. R., Weiss, R. F., Worthy, D., Wunch, D., Yin, Y., Yoshida, Y., Zhang, W., Zhang, Z., Zhao, Y., Zheng, B., Zhu,
695 Q., Zhu, Q., and Zhuang, Q.: The Global Methane Budget 2000-2017, *Earth Syst. Sci. Data Discuss.*, 2019, 1-138,
<https://doi.org/10.5194/essd-2019-128>, 2019.
- Schuur, E. A. G., McGuire, A. D., Schadel, C., Grosse, G., Harden, J. W., Hayes, D. J., Hugelius, G., Koven, C. D., Kuhry, P., Lawrence,
D. M., Natali, S. M., Olefeldt, D., Romanovsky, V. E., Schaefer, K., Turetsky, M. R., Treat, C. C., and Vonk, J. E.: Climate change and
the permafrost carbon feedback, *Nature*, 520, 171-179, <https://doi.org/10.1038/nature14338>, 2015.
- 700 Séférian, R., Rocher, M., Guivarch, C., and Colin, J.: Constraints on biomass energy deployment in mitigation pathways: the case of water
scarcity, *Environmental Research Letters*, 13, 054011, <https://doi.org/10.1088/1748-9326/aabcd7>, 2018.
- Shindell, D., Kuylenstierna, J. C. I., Vignati, E., van Dingenen, R., Amann, M., Klimont, Z., Anenberg, S. C., Muller, N., Janssens-Maenhout,
G., Raes, F., Schwartz, J., Faluvegi, G., Pozzoli, L., Kupiainen, K., Hoglund-Isaksson, L., Emberson, L., Streets, D., Ramanathan, V.,
Hicks, K., Oanh, N. T. K., Milly, G., Williams, M., Demkine, V., and Fowler, D.: Simultaneously Mitigating Near-Term Climate
705 Change and Improving Human Health and Food Security, *Science*, 335, 183-189, <https://doi.org/10.1126/science.1210026>, 2012.
- Sitch, S., Cox, P. M., Collins, W. J., and Huntingford, C.: Indirect radiative forcing of climate change through ozone effects on the land-
carbon sink, *Nature*, 448, 791-794, <https://doi.org/10.1038/nature06059>, 2007.
- Smith, P., Davis, S. J., Creutzig, F., Fuss, S., Minx, J., Gabrielle, B., Kato, E., Jackson, R. B., Cowie, A., Kriegler, E., van Vuuren, D. P.,
Rogelj, J., Ciais, P., Milne, J., Canadell, J. G., McCollum, D., Peters, G., Andrew, R., Krey, V., Shrestha, G., Friedlingstein, P., Gasser,
710 T., Grübler, A., Heidug, W. K., Jonas, M., Jones, C. D., Kraxner, F., Littleton, E., Lowe, J., Moreira, J. R., Nakicenovic, N., Obersteiner,
M., Patwardhan, A., Rogner, M., Rubin, E., Sharifi, A., Torvanger, A., Yamagata, Y., Edmonds, J., and Yongsung, C.: Biophysical and
economic limits to negative CO₂ emissions, *Nature Climate Change*, 6, 42, <https://doi.org/10.1038/nclimate2870>, 2016.
- Stehfest, E., van Vuuren, D., Kram, T., Bouwman, L., Alkemade, R., Bakkenes, M., Biemans, H., Bouwman, A., den Elzen, M., Janse, J.,
Lucas, P., van Minnen, J., Müller, C., and Prins, A.: Integrated Assessment of Global Environmental Change with IMAGE 3.0. Model
715 description and policy applications, PBL Netherlands Environmental Assessment Agency, The Hague, Netherlands. , Available from:
<http://www.pbl.nl/en/publications/integrated-assessment-of-global-environmental-change-with-IMAGE-3.0> (accessed November
2019), 2014.
- Stocker, T., Qin, D., Plattner, G., Tignor, M., Allen, S., Boschung, J., Nauels, A., Xia, Y., Bex, B., and Midgley, B.: The physical science
basis. Contribution of working group I to the fifth assessment report of the intergovernmental panel on climate change, in: IPCC, 2013:
720 Climate Change 2013, Cambridge University Press, 2013.

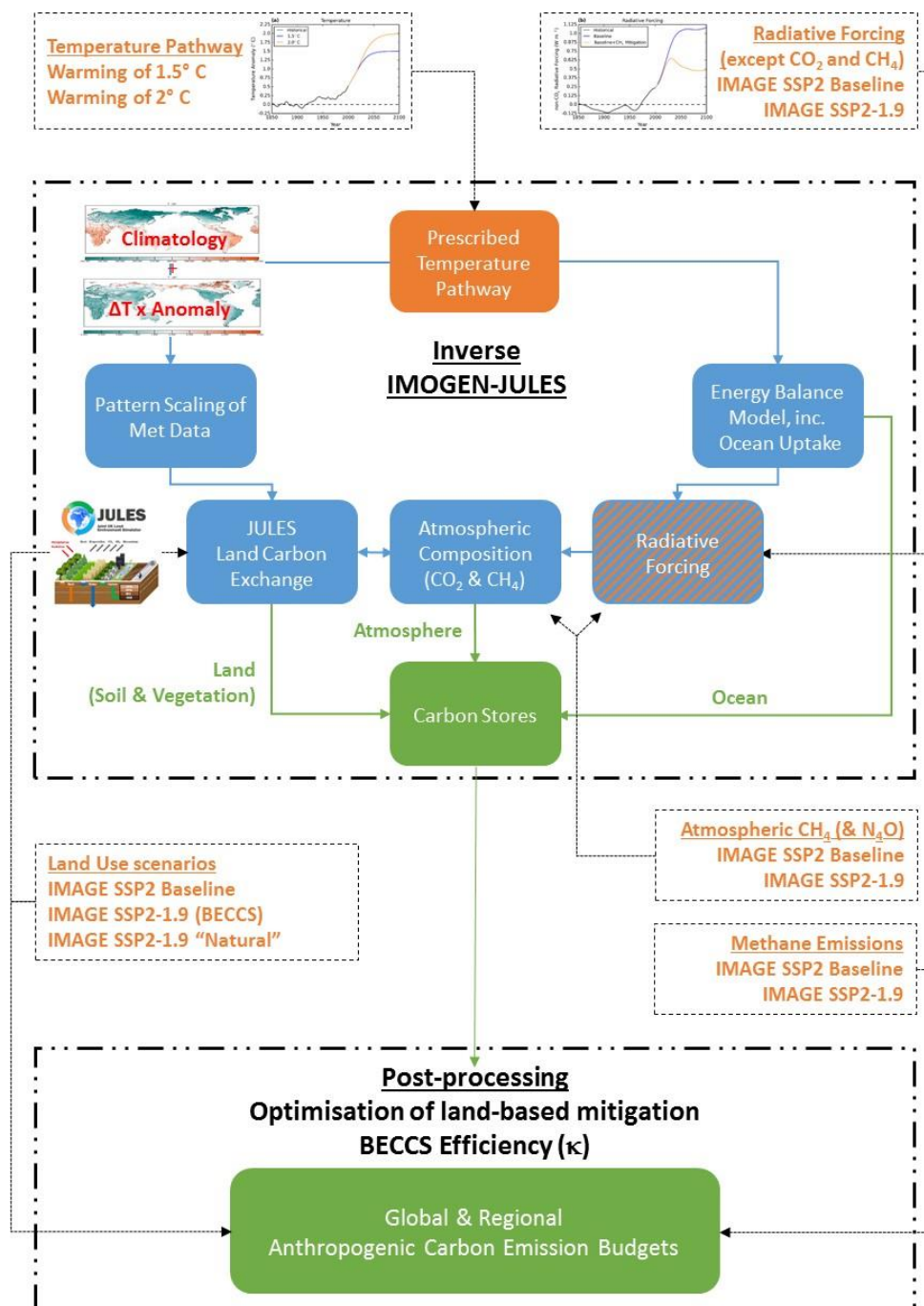


- 725 Stohl, A., Aamaas, B., Amann, M., Baker, L. H., Bellouin, N., Bernsten, T. K., Boucher, O., Cherian, R., Collins, W., Daskalakis, N.,
Dusinska, M., Eckhardt, S., Fuglestedt, J. S., Harju, M., Heyes, C., Hodnebrog, Ø., Hao, J., Im, U., Kanakidou, M., Klimont, Z.,
Kupiainen, K., Law, K. S., Lund, M. T., Maas, R., MacIntosh, C. R., Myhre, G., Myriokefalitakis, S., Olivie, D., Quaas, J., Quennehen,
B., Raut, J. C., Rumbold, S. T., Samset, B. H., Schulz, M., Seland, Ø., Shine, K. P., Skeie, R. B., Wang, S., Yttri, K. E., and Zhu, T.:
Evaluating the climate and air quality impacts of short-lived pollutants, *Atmos. Chem. Phys.*, 15, 10529-10566,
<https://doi.org/10.5194/acp-15-10529-2015>, 2015.
- 730 Turetsky, M. R., Kotowska, A., Bubier, J., Dise, N. B., Crill, P., Hornibrook, E. R. C., Minkinen, K., Moore, T. R., Myers-Smith, I. H.,
Nykanen, H., Olefeldt, D., Rinne, J., Saarnio, S., Shurpali, N., Tuittila, E.-S., Waddington, J. M., White, J. R., Wickland, K. P., and
Wilmking, M.: A synthesis of methane emissions from 71 northern, temperate, and subtropical wetlands, *Global Change Biology*, 20,
2183-2197, 10.1111/gcb.12580, 2014.
- UNFCCC: Adoption of the Paris Agreement, FCCC/CP/2015/L.9/Rev. 1, 2015.
- 735 van Vuuren, D. P., Stehfest, E., Gernaat, D. E. H. J., Doelman, J. C., van den Berg, M., Harmsen, M., de Boer, H. S., Bouwman, L. F.,
Daioglou, V., Edelenbosch, O. Y., Girod, B., Kram, T., Lassaletta, L., Lucas, P. L., van Meijl, H., Müller, C., van Ruijven, B. J., van
der Sluis, S., and Tabeau, A.: Energy, land-use and greenhouse gas emissions trajectories under a green growth paradigm, *Global
Environmental Change*, 42, 237-250, <https://doi.org/10.1016/j.gloenvcha.2016.05.008>, 2017.
- van Vuuren, D. P., Stehfest, E., Gernaat, D. E. H. J., van den Berg, M., Bijl, D. L., de Boer, H. S., Daioglou, V., Doelman, J. C., Edelenbosch,
O. Y., Harmsen, M., Hof, A. F., and van Sluisveld, M. A. E.: Alternative pathways to the 1.5 °C target reduce the need for negative
emission technologies, *Nature Climate Change*, 8, 391-397, <https://doi.org/10.1038/s41558-018-0119-8>, 2018.
- 740 Vaughan, N. E., and Gough, C.: Expert assessment concludes negative emissions scenarios may not deliver, *Environmental Research Letters*,
11, 095003, <https://doi.org/10.1088/1748-9326/11/9/095003>, 2016.
- Vaughan, N. E., Gough, C., Mander, S., Littleton, E. W., Welfle, A., Gernaat, D. E. H. J., and van Vuuren, D. P.: Evaluating the use of
biomass energy with carbon capture and storage in low emission scenarios, *Environmental Research Letters*, 13, 044014,
<https://doi.org/10.1088/1748-9326/aaaa02>, 2018.
- 745 Yamagata, Y., Hanasaki, N., Ito, A., Kinoshita, T., Murakami, D., and Zhou, Q.: Estimating water–food–ecosystem trade-offs for the global
negative emission scenario (IPCC-RCP2.6), *Sustainability Science*, 13, 301-313, <https://doi.org/10.1007/s11625-017-0522-5>, 2018.
- Zona, D., Gioli, B., Commane, R., Lindaas, J., Wofsy, S. C., Miller, C. E., Dinardo, S. J., Dengel, S., Sweeney, C., Karion, A., Chang, R.
Y.-W., Henderson, J. M., Murphy, P. C., Goodrich, J. P., Moreaux, V., Liljedahl, A., Watts, J. D., Kimball, J. S., Lipson, D. A., and
Oechel, W. C.: Cold season emissions dominate the Arctic tundra methane budget, *Proceedings of the National Academy of Sciences*,
113, 40-45, <https://doi.org/10.1073/pnas.1516017113>, 2016.

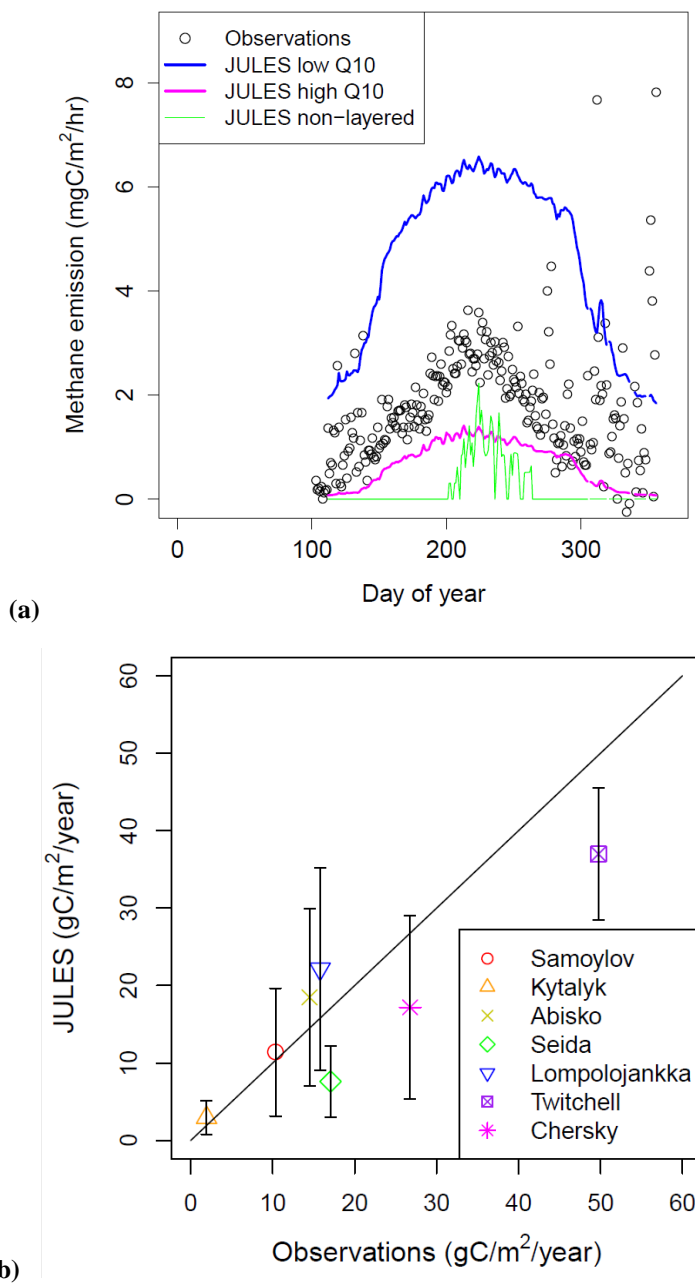
750



Figures



755 Figure 1 | Schematic of the modelling approach and the workflow. The coloured boxes and text show (a) the key components of the inverted IMOGEN-JULES model (blue), the prescribed data used in this study (orange) and the outputs (green).



760 **Figure 2 | (a) Observed (circles) and modelled wetland methane emissions at the Samoylov Island field site. Modelled wetland**
methane emissions are shown for the standard JULES non-layered soil carbon configuration (green) and for the JULES layered soil
carbon configurations with the low (blue line) and high (magenta line) Q₁₀ temperature sensitivities; the low Q₁₀ configuration gives
higher methane emissions at high-latitude sites such as the Samoylov Island field site. The methane emission data is preliminary and
was provided by Lars Kutzbach and David Holl. (b) Comparison of observed and modelled annual mean wetland CH₄ emission
765 **fluxes at a number of northern high-latitude and temperate sites.**

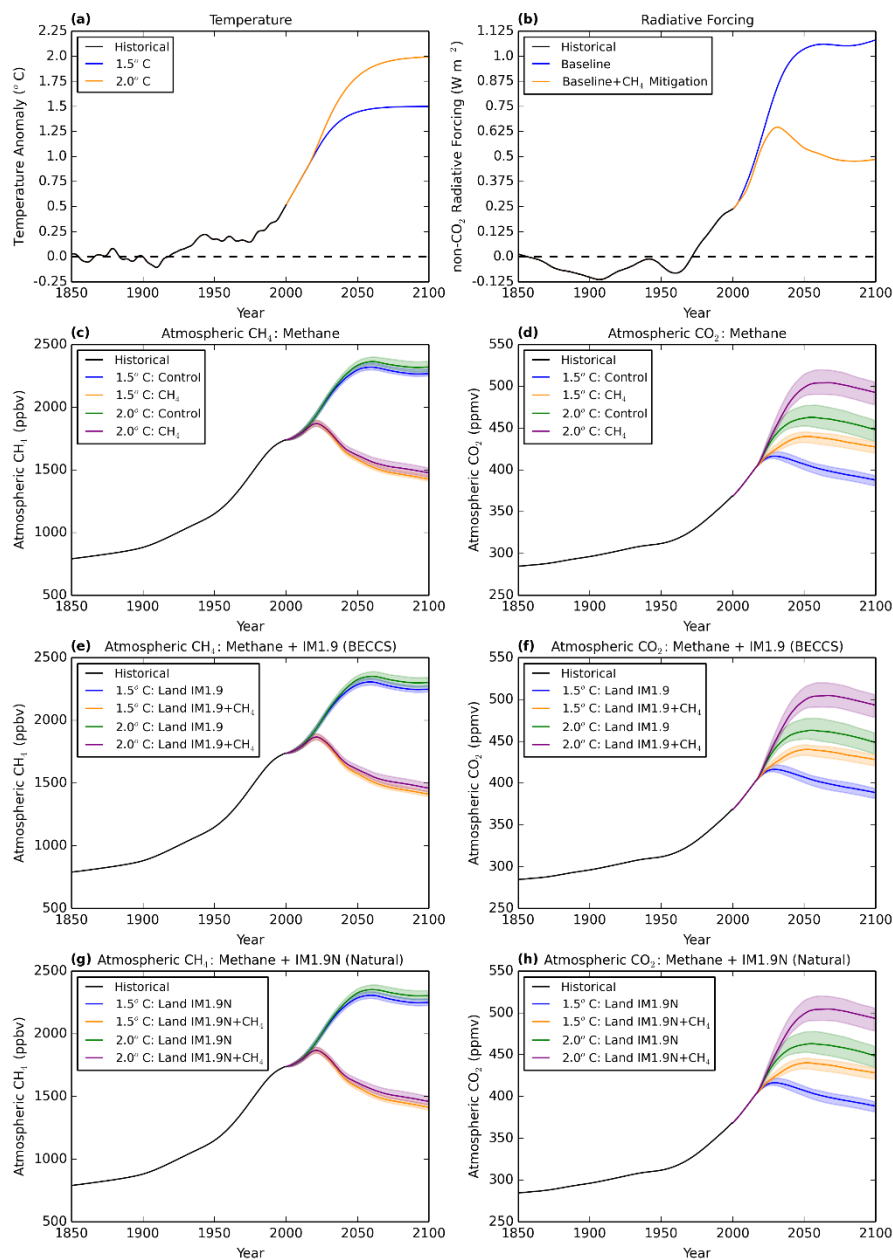
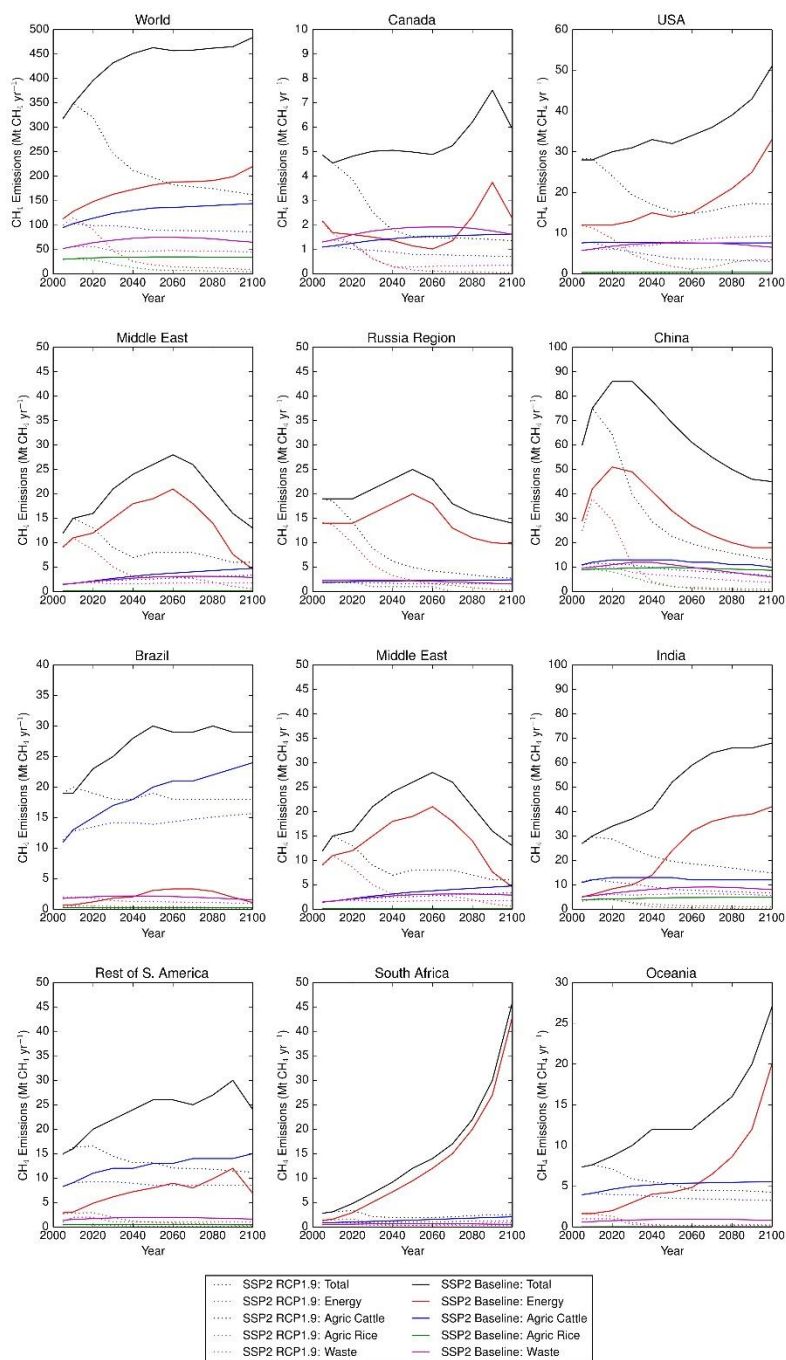
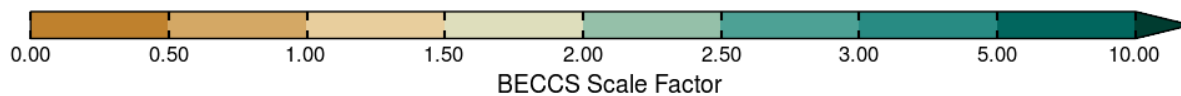
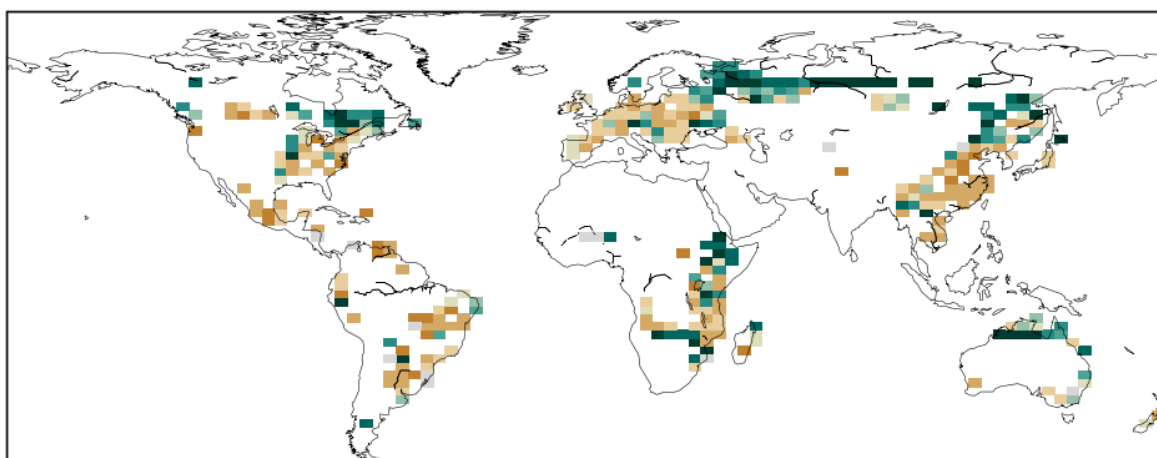


Figure 3 | Time series of (a) the temperature profiles used to represent warming of 1.5°C (blue) and 2°C (red); (b) the non-CO₂ greenhouse gas radiative forcing (W m⁻²) for the baseline (red) and methane mitigation (blue) scenarios; (c, e, f) the ensemble median atmospheric CH₄ concentrations (with interquartile range as spread) derived for each land use scenario: (c) IM-BL, (e) IM 1.9, (g) IM-1.9N. In each panel, time series are shown for the baseline (IM-BL) and methane mitigation (IM1.9) scenarios for each temperature profile. (d, f, h) the corresponding time series for the atmospheric CO₂ concentrations.

770

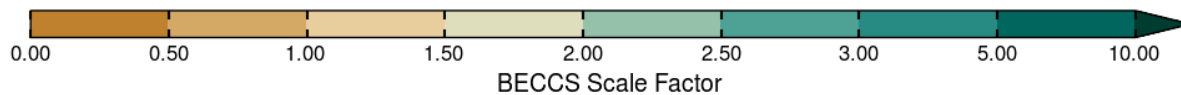
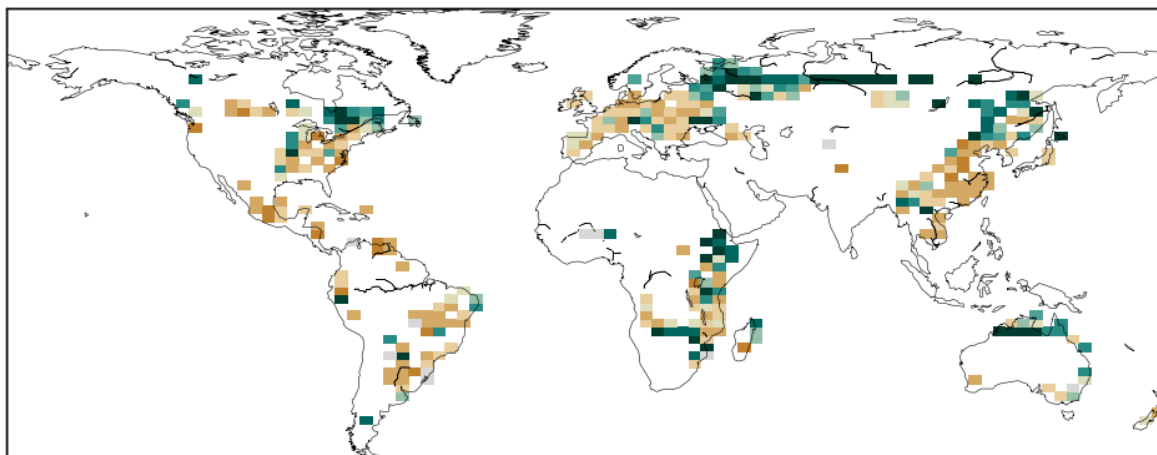


775 **Figure 4 | Time series of annual methane emissions between 2005 and 2100 from all and selected anthropogenic sources according to the IMAGE SSP2 Baseline (solid lines) and SSP2-RCP1.9 (dotted lines) scenarios, globally and for selected IMAGE regions, with total emissions in black, energy sector in red, agriculture-cattle in blue, agriculture-rice in green and waste in magenta. Note the y-axes have different scales for clarity.**



780

(b)

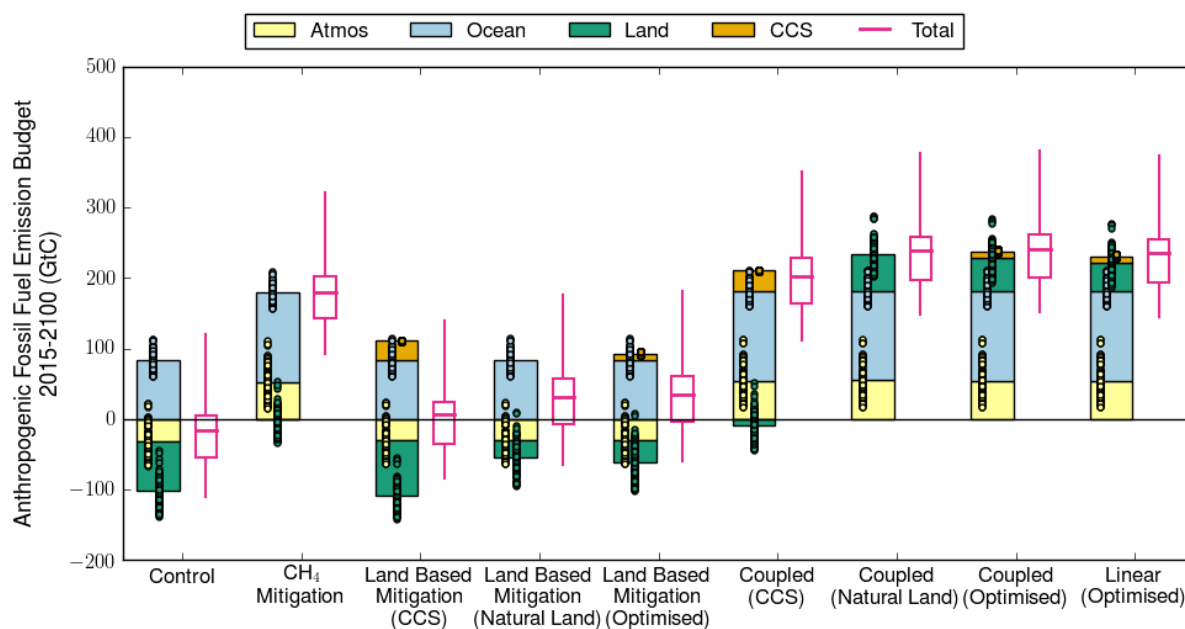


785

Figure 5 | Scale factor required for BECCS to be the preferable mitigation option, as opposed to natural land carbon uptake. The data represents the median of the 136 member ensemble for the optimised land-based mitigation simulation. Panel (a) is for stabilisation at 1.5°C and panel (b) is for stabilisation at 2°C.

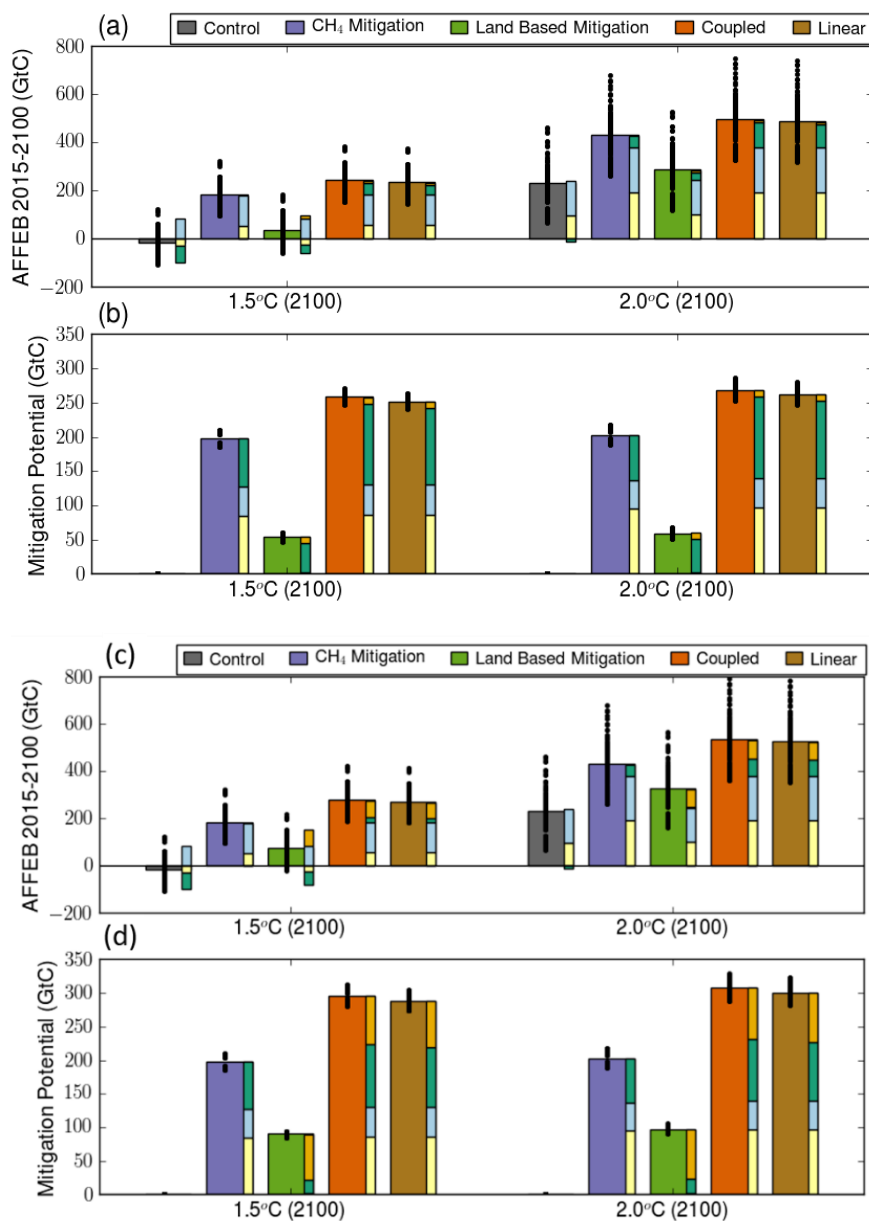


790



795

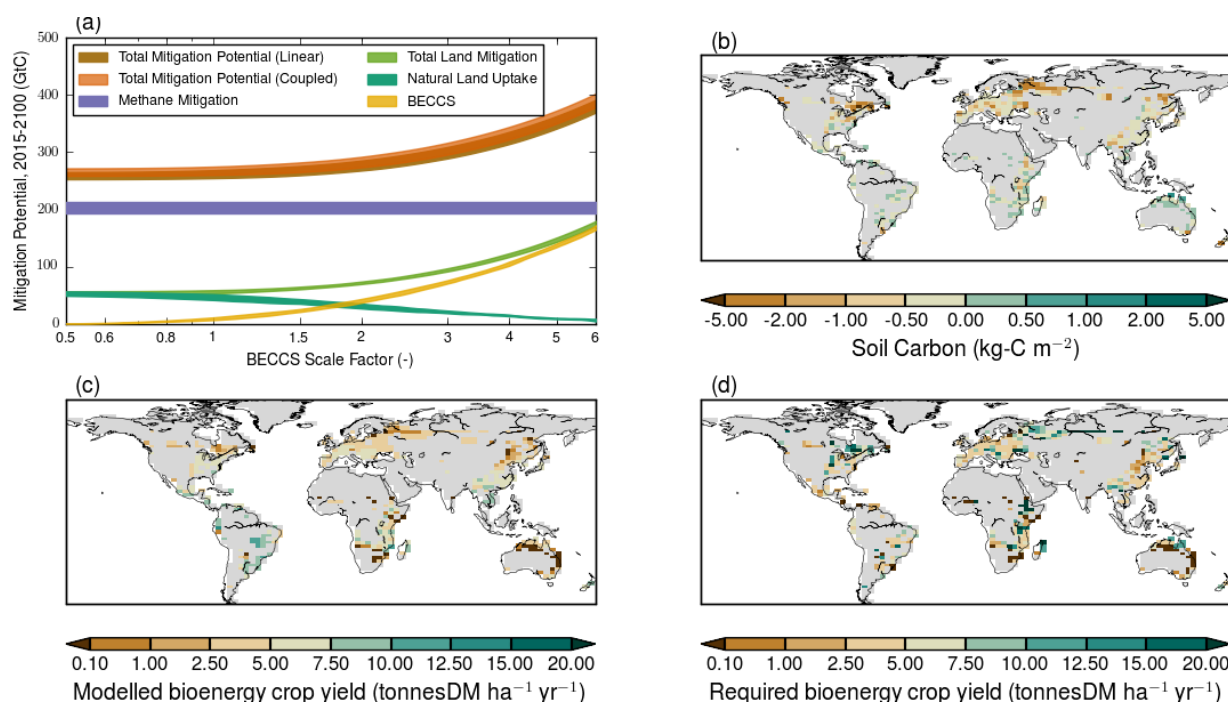
Figure 6 | The contribution to the allowable anthropogenic fossil fuel emission budget (AFFEBs, GtC) from the changes in the different carbon stores (atmosphere, ocean, land and BECCS) for the various control and mitigation runs, illustrated using the temperature pathways reaching 1.5°C without overshoot. The optimised land based and coupled mitigation options selects the land use option, which maximises the AFFEB for each model grid cell.



800
 805 **Figure 7 | Allowable anthropogenic fossil fuel emission budgets and mitigation potential for the factorial simulation experiment. (a & c) The allowable anthropogenic fossil fuel emission budgets (AFFEBs; GtC) for the control (grey), methane mitigation (purple), land-based mitigation (green), coupled methane and land-based mitigation (orange) and the linearly summed methane and land-based mitigation (brown), for 2 temperature pathways asymptoting at 1.5°C (left) and 2.0°C (right). (b & d) The mitigation potential (GtC) as the increase in AFFEB from the corresponding control run. a & b are for the standard JULES BECCS productivity and efficiency ($\kappa=1$, Sect. 2.4.3), in c & d the BECCS productivity and efficiency uses $\kappa=3$. The breakdown of the AFFEB and mitigation potential by the changes in the carbon stores: atmosphere (pale yellow), ocean (light blue), land (dark green) and BECCS (gold) is included alongside each bar.**



810



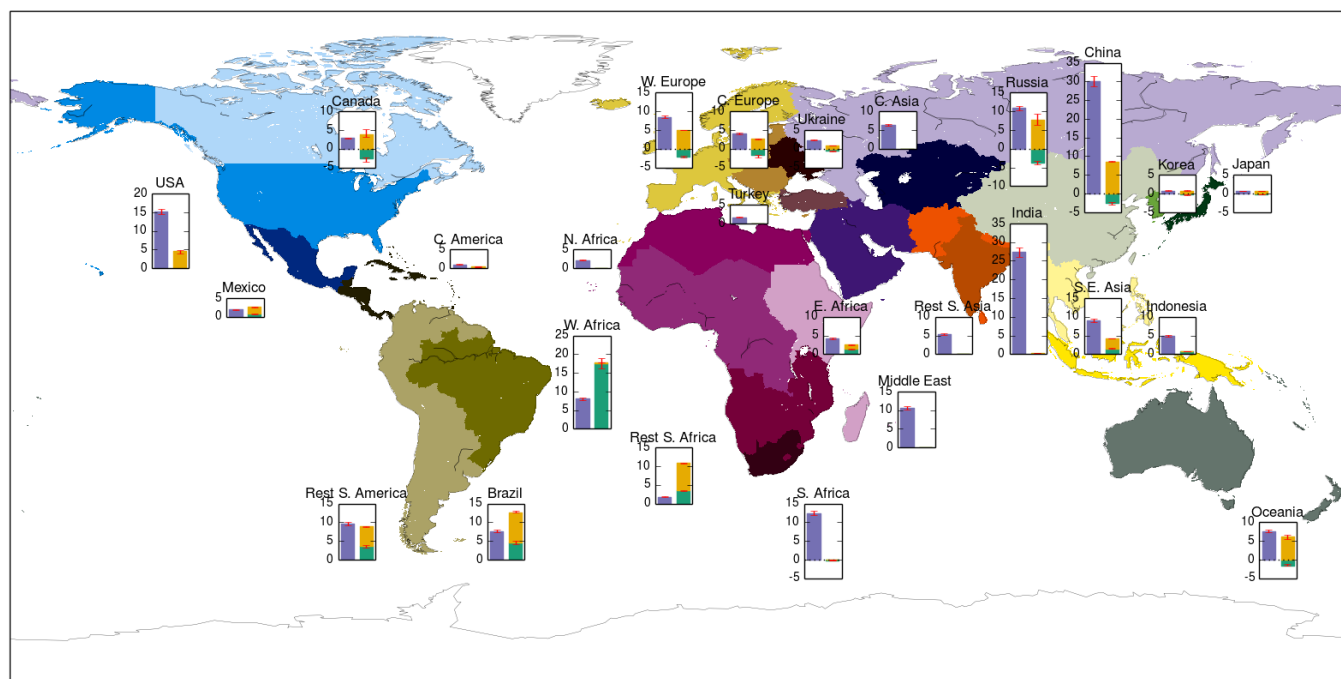
815

Figure 8| (a) The total and component mitigation potential (GtC) for different mitigation options, involving methane and land use, as a function of the BECCS efficiency factor (κ , Sect. 2.4.3) for the temperature pathway reaching 1.5°C. The spread of the functions represent the interquartile range of the sensitivity ensemble. Maps of (b) the change of the modelled soil carbon (kg-C m⁻²) between 2015 and 2099, as the difference between the scenario with BECCS and the natural land-management scenario; (c) the modelled mean bioenergy crop yield in the JULES simulations ($\kappa = 1$) and (d) the required bioenergy crop yield for BECCS to provide a larger carbon uptake than forest regrowth/afforestation (assuming $\kappa = \kappa^*$ and 87% efficiency of BECCS). Grid cells which do not exceed 1% BECCS cover for any year in the simulation are masked grey.

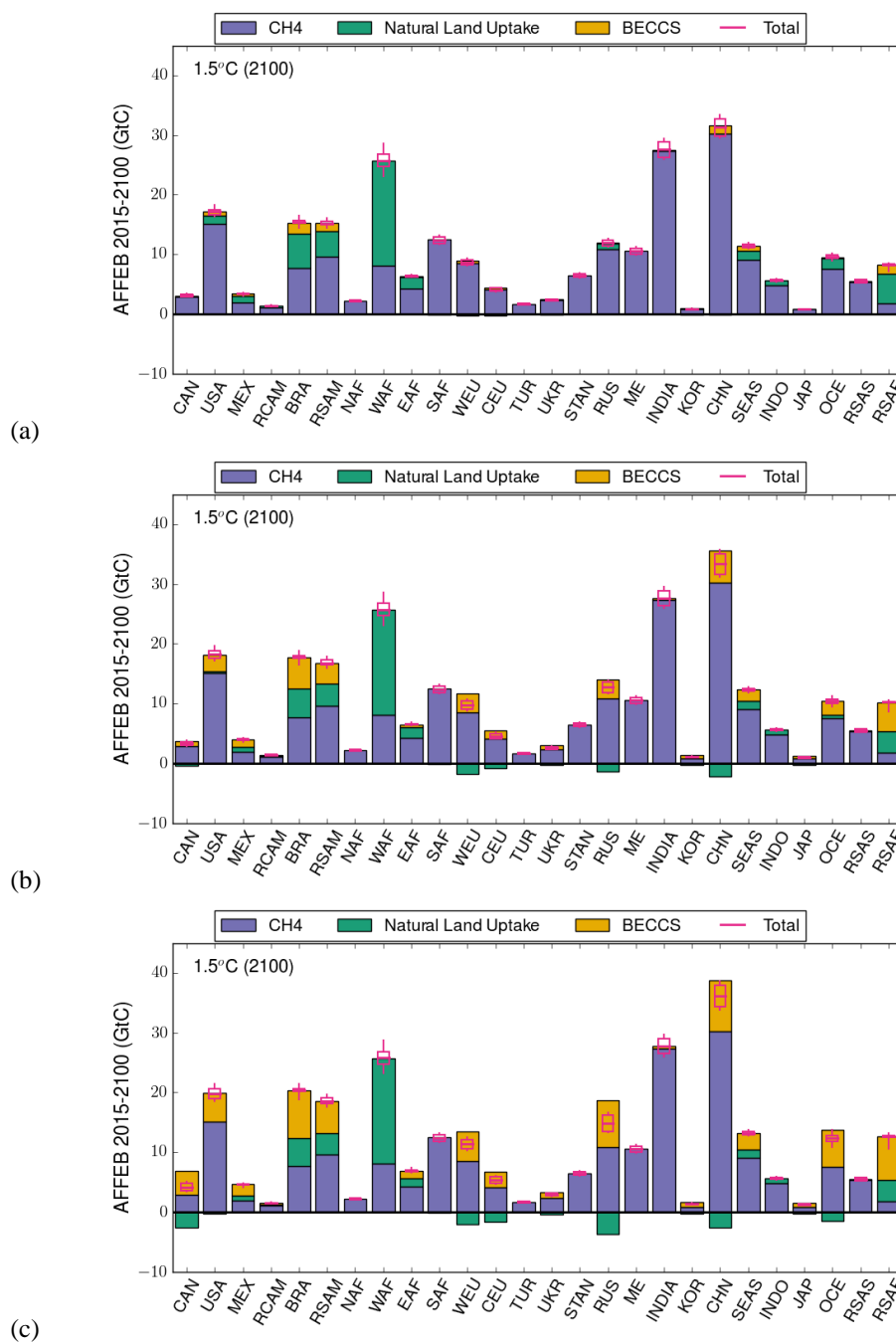
820



825



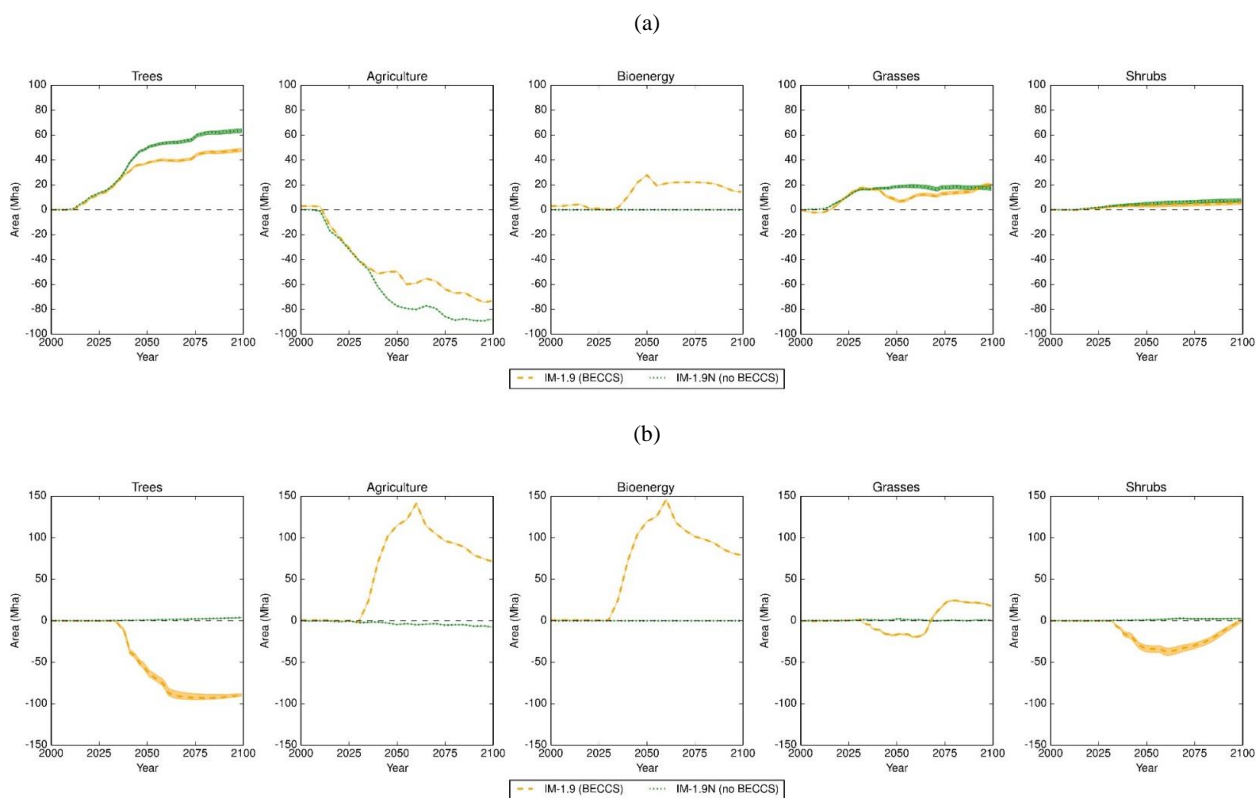
830 **Figure 9** | The contribution to the allowable carbon emission budgets (GtC) between 2015 and 2100 for each of the 26 IMAGE IAM regions from methane mitigation (purple bars) and land-based mitigation options (green: natural land uptake; yellow: BECCS with $\kappa = 3$), for the temperature pathway stabilising at 1.5° warming without overshoot. The bars and error bars respectively show the median and the interquartile range, from the 34 GCMs emulated and 4 factorial runs.



835

840

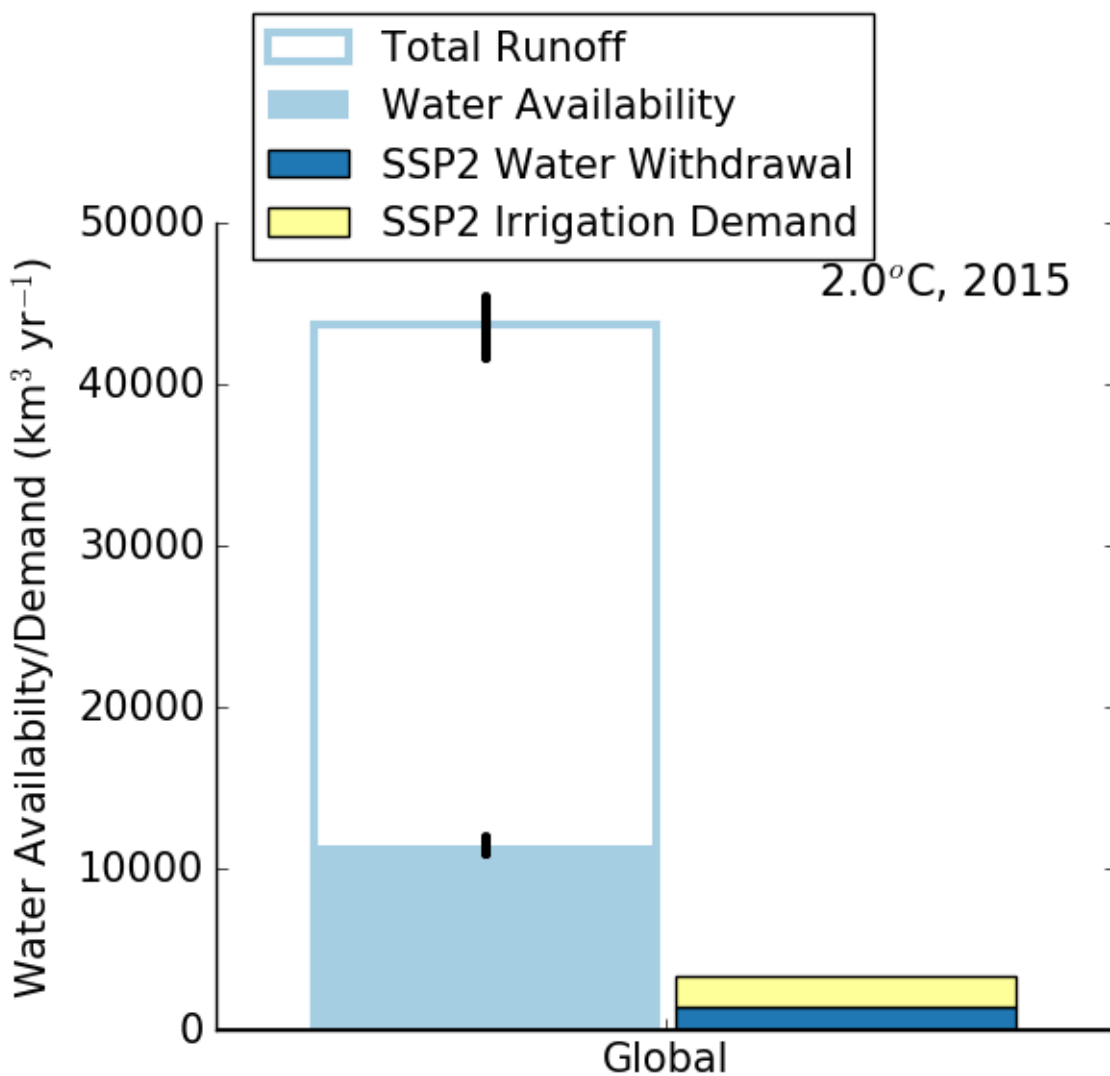
Figure 10 | Contribution of different mitigation options to the increase in allowable anthropogenic fossil fuel emission budgets by IMAGE region to meet the 1.5°C target. The stacked bars represent the median methane mitigation potential (purple bars) and median land-based mitigation potential (natural land uptake, green; BECCS, brown). Panel (a) is based on a BECCS scaling factor of unity, (b) a BECCS scaling factor of 2 and (c) a BECCS scaling factor of 3. The total (pink) shows the median and interquartile range for the 34 GCMs emulated and 4 factorial sensitivity simulations.



845

850

Figure 11 | Time series of the land areas (in Mha) calculated for trees and prescribed for agriculture (including bioenergy crops) and bioenergy crops for the scenarios IM-1.9 ('BECCS', orange) and IM-1.9N ('no BECCS', green), as a difference to the baseline scenario (IM-BL), for the Russia (panel a) and Brazil (panel b) IMAGE regions between 2000 and 2100. The dotted lines are the median and the spread the interquartile range for the 34 GCMs emulated and 4 factorial sensitivity simulations.



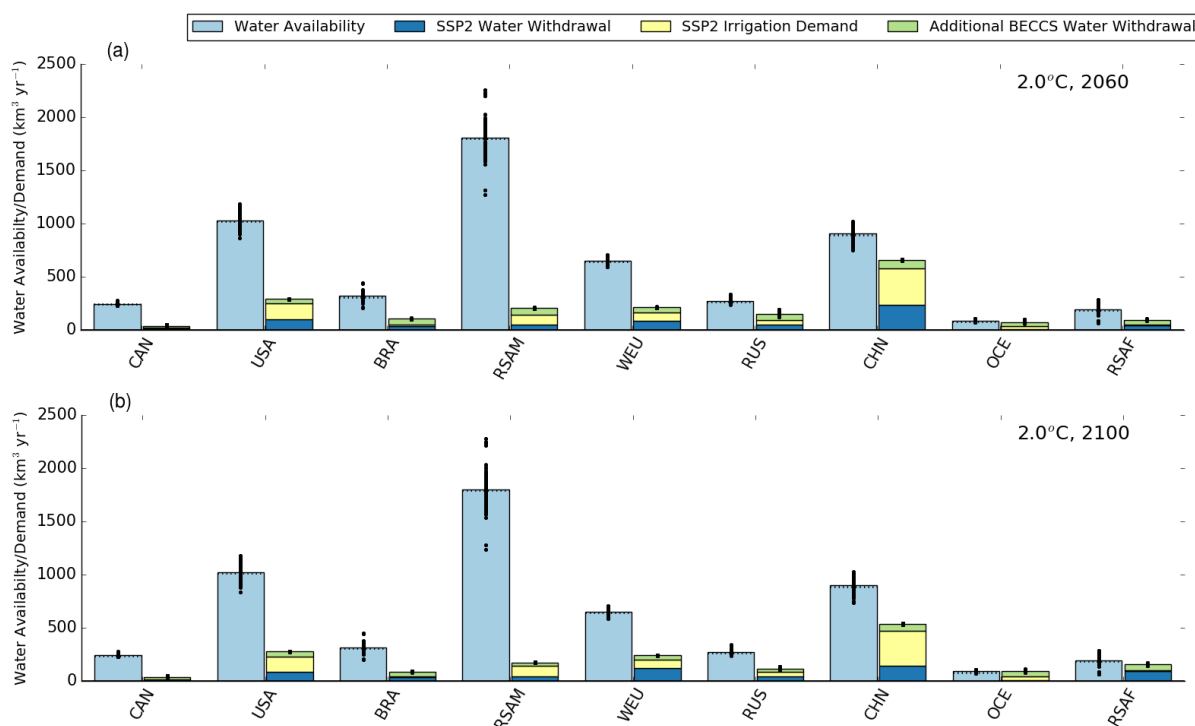
855

Figure 12 | Global water availability (filled light blue bar) as a regionally dependent fraction of runoff (hollow light blue bar) for the year 2015. The water withdrawal (dark blue) and irrigation demand are taken from the SSP2-RCP2.6-IMAGE database.



860

865



870

Figure 13 | Water availability (light blue), SSP2-IMAGE water demand estimates (dark blue) and the additional water demand from BECCS (green) for the years 2059-2060 and 2099-2100 for the 2.0°C warming target, with a BECCS κ factor of 3. The points are the individual results from the 34 GCMs emulated and 4 factorial runs, while the bars are the corresponding median values of the different GCM/factorial ensembles.



Tables

875

Table 1 | IMAGE regions, the maximum area of BECCS deployed (Mha) and the main differences in land use between the IM-1.9 and IM-1.9N scenarios.

Region	Abbreviation	Max. area of bioenergy crops (Mha)	Main land-use difference between IM-1.9 and IM-1.9N scenarios
Canada	CAN	65.9	Forest to BECCS in IM-1.9
USA	USA	39.0	Agricultural land and forest to BECCS (IM-1.9). Agricultural land to forest (IM-1.9N)
Mexico	MEX	7.1	Agricultural land to BECCS and forest (IM-1.9). Agricultural land to forest (IM-1.9N)
Central America	RCAM	0.5	Little BECCS. Agricultural land to forests in both scenarios.
Brazil	BRA	27.8	Agricultural land to BECCS and forest (IM-1.9). Agricultural land to forest (IM-1.9N)
Rest of South America	RSAM	20.3	Agricultural land to BECCS and forest (IM-1.9). Agricultural land to forest (IM-1.9N)
Northern Africa	NAF	0.0	No BECCS. No real differences between scenarios
Western Africa	WAF	3.1	Little BECCS. Agricultural land to forests in both scenarios.
Eastern Africa	EAF	33.9	Agricultural land to BECCS and forest (IM-1.9). Agricultural land to forest (IM-1.9N)
South Africa	SAF	1.0	Little BECCS. Agricultural land to forests in both scenarios.
Rest of Southern Africa	RSAF	63.7	Agricultural land to BECCS and forest (IM-1.9). Agricultural land to forest (IM-1.9N)
Western Europe	WEU	23.6	Forest to BECCS in IM-1.9
Central Europe	CEU	19.3	Forest to BECCS in IM-1.9
Turkey	TUR	0.0	No BECCS. No real differences between scenarios
Ukraine Region	UKR	11.4	Forest to BECCS in IM-1.9
Central Asia	STAN	0.7	Little BECCS. No real differences between scenarios
Russia Region	RUS	146.1	Forest to BECCS in IM-1.9
Middle East	ME	0.0	No BECCS. No real differences between scenarios
India	INDIA	6.0	Forest to BECCS in IM-1.9
Korea Region	KOR	4.3	Forest to BECCS in IM-1.9
China	CHN	58.1	Forest to BECCS in IM-1.9
South East Asia	SEAS	24.5	Forest to BECCS in IM-1.9. Agricultural land to forest (IM-1.9N)
Indonesia	INDO	0.0	No BECCS. Agricultural land to forests in both scenarios.
Japan	JAP	2.7	Forest to BECCS in IM-1.9
Rest of South Asia	RSAS	0.0	No BECCS. No real differences between scenarios
Oceania	OCE	78.7	Forest to BECCS in IM-1.9



880 Table 2 | The IMOGEN-JULES factorial runs, key features and IMAGE prescribed datasets.

Factorial Run	Abbreviation
1. Control: <ul style="list-style-type: none"> • IMAGE SSP2 baseline scenario • Agricultural land accrued to feed growing populations associated with the SSP2 pathway. No deployment of BECCS • Anthropogenic CH₄ emissions rise from 318 Tg per annum in 2005 to 484 Tg per annum in 2100 • IMAGE SSP2 baseline scenario for atmospheric concentrations of CH₄ and non-CO₂ radiative forcing 	CTL
2. Methane mitigation: <ul style="list-style-type: none"> • IMAGE SSP2 RCP1.9 scenario for CH₄ • Agricultural land-use as in Control • Anthropogenic CH₄ emissions decline from 318 Tg per annum in 2005 to 162 Tg per annum in 2100 • IMAGE SSP2-1.9 scenario for atmospheric concentrations of CH₄ and non-CO₂ radiative forcing 	CH ₄
3. Land-based mitigation, including BECCS: <ul style="list-style-type: none"> • Land use from IMAGE SSP2 RCP1.9 scenario • High levels of REDD and full reforestation • Food-first policy so that bioenergy crops are only implemented on land not required for food production • Anthropogenic CH₄ emissions as in Control • IMAGE SSP2 baseline scenario for atmospheric concentrations of CH₄ and non-CO₂ radiative forcing 	CCS
4. Land-based mitigation with no BECCS (Natural): <ul style="list-style-type: none"> • As 3, except any land allocated to bioenergy crops is set to zero, allowing expansion of natural vegetation • Anthropogenic CH₄ emissions as in Control • IMAGE SSP2 baseline scenario for atmospheric concentrations of CH₄ and non-CO₂ radiative forcing 	Natural Land
5. Combined methane & land-based mitigation: <ul style="list-style-type: none"> • Combines CH₄ mitigation of 2 with land-based mitigation of 3 • IMAGE SSP2-1.9 scenario for atmospheric concentrations of CH₄ and non-CO₂ radiative forcing 	Coupled (CH ₄ +CCS)
6. Combined methane & land-based mitigation with no BECCS (Natural) <ul style="list-style-type: none"> • Combines CH₄ mitigation of 2 with land use scenario of 4 • IMAGE SSP2-1.9 scenario for atmospheric concentrations of CH₄ and non-CO₂ radiative forcing 	Coupled (CH ₄ +Natural Land)

Note: Each factorial run comprises a 136-member ensemble: 34 GCMs x 2 ozone damage sensitivities x 2 methanogenesis Q₁₀ temperature sensitivities.



885

Table 3 | IMAGE regions and the projected accumulated anthropogenic CH₄ emissions (2020-2100) for the SSP2-Baseline and SSP2-RCP1.9 scenarios. The regional scale factor is calculated as the regional fraction of the global difference in anthropogenic CH₄ emissions (2020-2100).

Region	Abbreviation	Projected Anthropogenic CH ₄ Emissions 2020-2100 (PgCH ₄)		Difference	Scale Factor
		SSP2-Baseline	SSP2-RCP1.9		
Canada	CAN	0.497	0.169	0.328	0.01471
USA	USA	3.281	1.573	1.708	0.07670
Mexico	MEX	0.542	0.320	0.222	0.00995
Central America	RCAM	0.312	0.195	0.117	0.00525
Brazil	BRA	2.502	1.638	0.865	0.03884
Rest of South America	RSAM	2.249	1.159	1.090	0.04896
Northern Africa	NAF	0.533	0.286	0.247	0.01110
Western Africa	WAF	2.035	1.128	0.907	0.04074
Eastern Africa	EAF	1.722	1.245	0.478	0.02146
South Africa	SAF	1.615	0.207	1.408	0.06324
Rest of Southern Africa	WEU	1.883	0.924	0.959	0.04307
Western Europe	CEU	0.683	0.220	0.463	0.02081
Central Europe	TUR	0.409	0.219	0.190	0.00854
Turkey	UKR	0.387	0.128	0.259	0.01163
Ukraine Region	STAN	1.021	0.299	0.722	0.03241
Central Asia	RUS	1.743	0.514	1.228	0.05517
Russia Region	ME	1.910	0.720	1.190	0.05343
Middle East	INDIA	4.873	1.788	3.085	0.13856
India	KOR	0.170	0.081	0.089	0.00400
Korea Region	CHN	5.757	2.351	3.406	0.15296
China	SEAS	1.923	0.908	1.015	0.04558
South East Asia	INDO	1.005	0.457	0.547	0.02458
Indonesia	JAP	0.160	0.077	0.082	0.00369
Japan	OCE	1.316	0.460	0.856	0.03846
Rest of South Asia	RSAS	1.496	0.893	0.603	0.02710
Oceania	RSAF	0.657	0.455	0.202	0.00907
World	World	40.680	18.415	22.265	1.00000

890



Table 4 | Projected total anthropogenic water withdrawals ($\text{km}^3 \text{ yr}^{-1}$) and irrigation demand for the years 2060, 2100 by IMAGE region from the IMAGE SSP2-RCP2.6 scenario and percentage of runoff available for human use.

Region	Abbreviation	Projected Water Withdrawals ($\text{km}^3 \text{ yr}^{-1}$)		Projected Irrigation Demand ($\text{km}^3 \text{ yr}^{-1}$)		% of Runoff Available
		2060	2100	2060	2100	
Canada	CAN	14.21	11.72	3.39	4.31	5 %
USA	USA	96.07	81.35	149.55	148.57	40 %
Mexico	MEX	25.56	23.78	76.58	77.27	40 %
Central America	RCAM	15.49	13.96	8.16	8.74	40 %
Brazil	BRA	34.44	30.80	12.24	12.31	5 %
Rest of South America	RSAM	46.49	38.34	93.50	103.97	40 %
Northern Africa	NAF	54.63	56.98	61.60	57.89	40 %
Western Africa	WAF	118.83	262.07	28.29	37.23	40 %
Eastern Africa	EAF	63.10	128.33	53.92	58.96	40 %
South Africa	SAF	9.28	7.50	13.45	13.43	40 %
Rest of Southern Africa	RSAF	82.01	118.64	78.72	80.39	40 %
Western Europe	WEU	22.32	20.63	27.46	26.90	40 %
Central Europe	CEU	15.86	12.87	60.35	60.49	40 %
Turkey	TUR	25.90	19.58	11.73	10.40	40 %
Ukraine Region	UKR	32.62	37.90	88.26	82.08	40 %
Central Asia	STAN	51.60	43.82	42.30	40.25	40 %
Russia Region	RUS	40.97	39.30	149.55	136.63	5 %
Middle East	ME	501.06	585.48	374.18	388.69	40 %
India	INDIA	9.75	5.47	6.20	7.41	40 %
Korea Region	KOR	236.89	144.80	338.81	326.62	40 %
China	CHN	92.99	131.95	46.52	45.46	40 %
South East Asia	SEAS	113.87	114.33	8.18	15.08	40 %
Indonesia	INDO	18.99	13.29	2.79	2.12	40 %
Japan	JAP	8.91	8.77	24.99	30.57	40 %
Rest of South Asia	RSAS	154.42	227.85	259.95	245.78	40 %
Oceania	OCE	41.36	89.87	10.03	11.20	40 %
World	World	1927.62	2269.39	2030.70	2032.74	